Photon-odderon interference in exclusive χc charmonium production at the Electron-Ion Collider

Benić, Sanjin; Dumitru, Adrian; Kaushik, Abhiram; Motyka, Leszek; Stebel, Tomasz

Photon-odderon interference in exclusive χ_c charmonium production at the Electron-Ion Collider

Sanjin Benić,[1] Adrian Dumitru,[2,3] Abhiram Kaushik,[4] Leszek Motyka,[5] and Tomasz Stebel[5]

[1]*Department of Physics, Faculty of Science, University of Zagreb, Bijenička c. 32, 10000 Zagreb, Croatia*
[2]*Department of Natural Sciences, Baruch College, CUNY, 17 Lexington Avenue,
New York, New York 10010, USA*
[3]*The Graduate School and University Center, The City University of New York,
365 Fifth Avenue, New York, New York 10016, USA*
[4]*Centre for Informatics and Computing, Rudjer Bošković Institute, HR-10002 Zagreb, Croatia*
[5]*Jagiellonian University, Institute of Theoretical Physics, Łojasiewicza 11, 30-348 Kraków, Poland*

Exclusive $C = +1$ scalar, axial-vector, and tensor quarkonium production in high-energy electron-proton scattering requires a C-odd t-channel exchange of a photon or a three-gluon ladder. We derive the expressions for the corresponding amplitudes. The relative phase of the photon vs three-gluon exchange amplitudes is determined by the sign of the light-front matrix element of the eikonal color current operator $d^{abc}J^{+a}J^{+b}J^{+c}$ at moderate x, and is not affected by small-x QCD evolution. Model calculations predict constructive interference, which is particularly strong for momentum transfer $|t| \sim 1$ GeV^2 where the cross section for χ_{cJ} production exceeds that for pure photon exchange by up to a factor of 4. Exclusive χ_{cJ} electroproduction at the high luminosity Electron-Ion Collider occurs with well measurable rates and measurements of these processes should find evidence for the perturbative odderon exchange. We also compute the total electroproduction cross section as a function of energy and provide first estimates of the number of χ_{cJ} events per month at the Electron-Ion Collider design luminosity.

I. INTRODUCTION

A basic prediction of QCD, related to the nonzero cubic Casimir invariant, is that there exists a contribution to high-energy scattering amplitudes from a C-conjugation odd exchange driven mostly by gluons, with a weakly energy dependent cross section. The possible existence of such an exchange, called the odderon, was predicted 50 years ago from general principles of quantum field theory [1]. If the scattering involves hadrons of a size much smaller than the QCD confinement scale, or high momentum transfer, then the composition of the exchanged "state" can be understood from perturbative QCD. At leading order in perturbation theory, it corresponds to an exchange of three gluons which is symmetric under permutations of their colors. At high energies the three-gluon exchange is dressed by higher order QCD corrections enhanced by logarithms of energy that have to be resummed into a gluon ladder. It accounts for interactions between the exchanged t-channel gluons, and for virtual corrections. The resulting "Reggeized"

three-gluon exchange is the hard odderon. In the weak field limit the corresponding Bartels–Jaroszewicz–Kwieciński–Praszałowicz (BJKP) linear QCD evolution equation has been obtained long ago [2–4], and it amounts to the Reggeization of the exchanged gluons by iteration of the Balitsky–Fadin–Kuraev–Lipatov (BFKL) interaction kernel [5–7] for each pair of gluons in the ladder. The NLO corrections to the BJKP equation were found in Ref. [8]. At asymptotically high energies the leading solution to the BJKP equation corresponds to a configuration of gluons in which two Reggeized gluons are combined together [9]—the Bartels–Lipatov–Vacca (BLV) solution. The BLV solution couples to color dipoles so it is particularly important in C-even quarkonia (or meson) photo- and electroproduction [9]. The intercept of this solution equals one, in the leading logarithmic approximation [9], and it was argued that it remains at this value to all orders in the perturbative expansion [10].

The nonlinear odderon evolution equation for dipole-proton scattering was established in Refs. [11,12]. This equation typically produces solutions where the odderon amplitude decreases with energy [13–17], as will be confirmed also in our present work. The seed for this evolution to small x is provided by the cubic Casimir $d^{abc}J^{+a}J^{+b}J^{+c}$ in the effective action describing color

current (J^{+a}) fluctuations in the proton at moderately small x [18,19], which allows the C-odd gluon ladder to couple to the proton. The matrix element[1] of this operator could also be evaluated directly from the light-cone wave function of the proton [23,24]. A key point for the present analysis is that the odderon evolution equation to small x *does not alter the sign* of the amplitude. Hence, the interference pattern with the electromagnetic amplitude due to single photon exchange is determined by the sign of the matrix element of the $d^{abc}J^{+a}J^{+b}J^{+c}$ operator at the initial, moderately small x.

TOTEM collaboration at CERN-LHC has measured the differential cross section for pp elastic scattering at $\sqrt{s} = 2.76$ GeV [25]. They observe a significant difference to the cross section for $p\bar{p}$ scattering at $\sqrt{s} = 1.96$ GeV measured by D0 [26]. Assuming that the difference in energy is negligible they conclude that these results provide evidence for the exchange of a color singlet gluonic state with odd C-parity, the odderon. However, these measurements involve the scattering of hadrons with a size of order the QCD confinement scale as well as low momentum transfers, $|t| \ll 1$ GeV^2. Hence, an analysis of the nature of the t-channel exchange from perturbative QCD would not appear reliable.

Exclusive production of pseudoscalar η_c quarkonia in DIS has previously been proposed as a process suitable for the discovery of the hard odderon exchange in QCD [17,27–33]. In practice, the detection of this process is difficult as the η_c has small branching ratios to all relevant decay channels. For example, the radiative $\eta_c \to \gamma\gamma$ mode has a tiny ($\sim 10^{-4}$) branching ratio,[2] while the hadronic $\eta_c \to \rho\rho$ mode has a branching ratio of 1.5%. Also, the cross section for exclusive production of J/ψ is expected to be far greater than that for η_c, and so most η_c's would originate from a $J/\psi \to \eta_c\gamma$ decay.[3] The experimental identification of the soft photon ($M_{J/\psi} = 3.097$ GeV, $M_{\eta_c} = 2.984$ GeV) is difficult [35,36].

Alternative approaches for the discovery of the hard odderon include Pomeron–odderon interference (with a background from Pomeron–photon interference) which would manifest in asymmetries in exclusive production of two charged particles in DIS [37–39]; for the $\gamma^* p \to \chi_c p$ process considered here, it is instead the interference of the Primakoff-like amplitude with the QCD odderon exchange

amplitude which will be important, i.e., photon-odderon interference. Another process which involves a C-odd t-channel gluonic exchange is exclusive production of a J/ψ in double-diffractive proton-proton scattering [40,41]. At high-energy proton colliders this requires instrumentation over a large range of rapidity, close to the beams.

GlueX Collaboration at Jefferson Lab has recently reported the observation of 56.5 ± 8.2 exclusive $\chi_{c1}(1P)$ and 12.7 ± 4.5 $\chi_{c2}(1P)$ production events near threshold energy [42]. They noticed a "dramatic difference" in the momentum transfer t-distribution of events as compared to J/ψ production in that the cross section for χ_c production appears to drop off much less rapidly with increasing $|t|$. In other words, the probability that the struck proton remains intact at high momentum transfer is much greater in $\gamma p \to \chi_c p$ than in $\gamma p \to J/\psi p$ events. This remarkable result illustrates the importance of the underlying QCD dynamics as opposed to naive expectations based solely on the mass of the produced quarkonia. A much harder t dependence for exclusive production of η_c vs J/ψ in eikonal dipole-proton scattering is predicted by simple light-front constituent quark models [33]. Inspired by the GlueX measurement of exclusive χ_c production in DIS at Jefferson Lab, here we consider the same process but at high energies appropriate for the future Electron-Ion Collider (EIC) [43,44] where dipole model factorization [45,46] applies, and where the t-channel exchange of a C-odd color singlet state dominates.

Within the χ_{cJ} family ($J = 0, 1, 2$), χ_{c1} has the largest branching ratio for the radiative $\chi_{c1} \to J/\psi\gamma$ decay (34.3% as opposed to 1.4% for χ_{c0} and 19.0% for χ_{c2}). Indeed, this was the detection channel used by the GlueX measurement. Therefore, the production of χ_{c1} axial-vector and χ_{c2} tensor quarkonia may prove the most promising channels for discovery of the hard odderon. This is further corroborated by the fact that for χ_{c1} and χ_{c2} the odderon and photon exchange contributions become comparable at lower $|t|$ than for χ_{c0}, within the acceptance of the proton spectrometer of the EIC design detector [44]. However, for the χ_{cJ} quarkonia there is again a feed-down channel from exclusive production of $\psi(2S)$ with subsequent decay $\psi(2S) \to \chi_{cJ}\gamma$. Hence, the identification and rejection of such feed down is required.

The paper is organized as follows. In Sec. II we start with the computation of the amplitude and the corresponding $\gamma^* p$ cross section for exclusive production of C-even scalar, axial-vector, and tensor quarkonia. We derive the light-cone wave functions of quarkonia, whereas the amplitude is obtained as an overlap with the photon light-cone wave function. We introduce the odderon exchange amplitude and discuss its evolution to small x. Section III is devoted to the computation of the Primakoff contribution, where we pay special attention to the $t \to 0$ limit. In Sec. IV we perform a numerical fit of the χ_{cJ} wave functions. The main results are shown in Sec. V, where we numerically compute exclusive $\gamma^* p \to \chi_{cJ} p$ and $ep \to \chi_{cJ} ep$ cross sections and the expected number of events at the EIC. Our findings are

---

[1]We are here concerned with the off-forward matrix element for nonzero momentum transfer t. In the $t \to 0$ limit, instead, the "spin dependent odderon" [20–22] is associated with a spin flip of the proton in DIS.

[2]We take all branching ratios and particle masses from the "Review of Particle Physics" [34].

[3]This issue could be mitigated by considering $\eta_c(2S)$ instead, since it lies between the J/ψ and the $\psi(2S)$. The branching ratio $\psi(2S) \to \eta_c + \gamma$ is favorably small (($7 \pm 5) \times 10^{-4}$) but the detection of the $\eta_c(2S)$ is again problematic due to the small branching ratios for many channels.

summarized in the final Sec. VI. Several Appendixes follow where we explain the computational steps leading to some of the results from the main text.

II. THE PRODUCTION AMPLITUDE OF C-EVEN QUARKONIA

We consider the process $\gamma^*(q)p(P) \rightarrow p(P')\mathcal{H}(\Delta)$ where $\mathcal{H}$ is a C-even quarkonium state, specifically a P-wave χ_{cJ} charmonium state with $J = 0, 1, 2$. However our derivations are presented in a general form so that they apply also to other $C = +1$ $q\bar{q}$ bound states such as bottomonia, or even mesons with light flavor content.

Our computation is performed in the dipole frame where $q = (-Q^2/2q^-, q^-, 0, 0)$, $P = (P^+, 0, 0, 0)$, and the proton mass $M_p \ll \sqrt{(q+P)^2}$ is neglected. We use the convention for the components (v^+, v^-, v^1, v^2) of a four-vector v where $v^\pm = (v^0 \pm v^3)/\sqrt{2}$ are the $\pm$ light-cone components. The amplitude is computed using light-cone gauge $A^- = A \cdot n = 0$, that is, $n^\mu = \delta^{\mu+}$, for the field corresponding to the incoming photon.

Following a similar procedure as in [17,33] our starting point is the amplitude

$$\langle \mathcal{M}_{\lambda\bar{\lambda}}(\gamma^* p \rightarrow \mathcal{H}p) \rangle$$
$$= 2q^- N_c \int_{r_\perp b_\perp} e^{-i\Delta_\perp \cdot b_\perp} i\mathcal{O}(r_\perp, b_\perp) \mathcal{A}_{\lambda\bar{\lambda}}(r_\perp, \Delta_\perp), \quad (1)$$

with λ and $\bar{\lambda}$ the helicities of the incoming photon and the outgoing quarkonium, respectively. For brevity, we will oftentimes write the amplitude simply as $\langle \mathcal{M}_{\lambda\bar{\lambda}} \rangle$ (omitting the round parenthesis). Here $\mathcal{A}_{\lambda\bar{\lambda}}(r_\perp, \Delta_\perp)$ is the reduced amplitude, described physically in terms of the photon ($\Psi^\gamma_{\lambda,h\bar{h}}$) and the quarkonium ($\Psi^{\mathcal{H}}_{\lambda,h\bar{h}}$) wave function overlap. We have[4]

$$\mathcal{A}_{\lambda\bar{\lambda}}(r_\perp, \Delta_\perp) = \int_z \int_{l_\perp l'_\perp} \sum_{h\bar{h}} \Psi^\gamma_{\lambda,h\bar{h}}(l_\perp, z) \Psi^{\mathcal{H}*}_{\bar{\lambda},h\bar{h}}(l'_\perp - z\Delta_\perp, z)$$
$$\times e^{i(l_\perp - l'_\perp + \frac{1}{2}\Delta_\perp) \cdot r_\perp}. \quad (2)$$

A particular contribution to the amplitude (1) is shown in Fig. 1, where the upper heavy quark loop represents the reduced amplitude $\mathcal{A}_{\lambda\bar{\lambda}}(r_\perp, \Delta_\perp)$, and the three-gluon contribution is the lowest order depiction of the odderon exchange amplitude $\mathcal{O}(r_\perp, b_\perp)$ for the particular case where the gluons connect to three different quarks in the proton wave function, represented by the green blob.

The photon wave-function in momentum space is given by

---

[4]We employ the following abbreviation for the transverse coordinate space integrals: $\int_{r_\perp} \equiv \int d^2 r_\perp$. For transverse and longitudinal momentum space integrals we use $\int_{l_\perp} \equiv \int d^2 l_\perp/(2\pi)^2$ and $\int_z \equiv \int_0^1 dz/(4\pi)$.
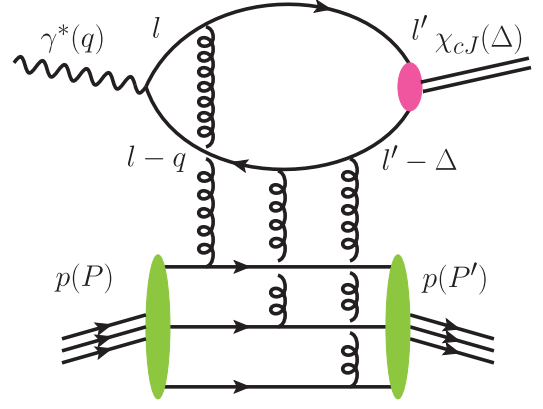

FIG. 1. An example Feynman diagram illustrating the amplitude for exclusive production of χ_{cJ}'s via three-gluon (odderon) exchange from the proton in $\gamma^* p$ collision. The green blobs represent the proton wave function that is shown here in terms of three valence quarks. The magenta blob is the χ_{cJ} wave function. In the dipole approach the two gluons coupling to the same quark line in the top part of the diagram occupy the same point in transverse position space.

$$\Psi^\gamma_{\lambda,h\bar{h}}(k_\perp, z) \equiv \sqrt{z\bar{z}} \frac{\bar{u}_h(k)eq_c\epsilon(\lambda,q)v_{\bar{h}}(q-k)}{k_\perp^2 + \varepsilon^2}, \quad (3)$$

where $q_c = +2/3$ is the fractional electric charge of the c-quark and $u_h(k)$ ($v_{\bar{h}}(q-k)$) are particle (antiparticle) spinors with $h = \pm 1$ indicating the sign of the helicity $h/2$. For explicit computations we use Lepage–Brodsky (LB) spinors [47]—see Appendix A for their expressions. $\epsilon(\lambda,q)$ is the photon polarization vector: we have $\epsilon(0,q) = (Q/q^-, 0, 0, 0)$ for longitudinal ($\lambda = 0$) and $\epsilon(\lambda,q) = (0, 0, \epsilon_\perp^\lambda)$ for transverse ($\lambda = \pm 1$) polarization. We follow the LB convention for the 2D polarization vector: $\epsilon_\perp^\lambda \equiv (-\lambda, -i)/\sqrt{2}$, and the common shorthands $\varepsilon \equiv \sqrt{m_c^2 + z\bar{z}Q^2}$ and $\bar{z} \equiv 1 - z$, with $z = k^-/q^-$. We compute the photon wave function as described in Appendix A, with the result

$$\Psi^\gamma_{+,h\bar{h}}(k_\perp, z) = -\sqrt{2}eq_c[k_\perp e^{i\phi_k}(z\delta_{h+}\delta_{\bar{h}-} - \bar{z}\delta_{h-}\delta_{\bar{h}+})$$
$$+ m_c\delta_{h+}\delta_{\bar{h}+}]\frac{1}{k_\perp^2 + \varepsilon^2},$$

$$\Psi^\gamma_{-,h\bar{h}}(k_\perp, z) = -\sqrt{2}eq_c[k_\perp e^{-i\phi_k}(\bar{z}\delta_{h+}\delta_{\bar{h}-} - z\delta_{h-}\delta_{\bar{h}+})$$
$$+ m_c\delta_{h-}\delta_{\bar{h}-}]\frac{1}{k_\perp^2 + \varepsilon^2},$$

$$\Psi^\gamma_{0,h\bar{h}}(k_\perp, z) = \frac{eq_c 2Qz\bar{z}}{k_\perp^2 + \varepsilon^2}\delta_{h,-\bar{h}}, \quad (4)$$

where $k_\perp e^{\pm i\phi_k} = k^1 \pm ik^2$. Equation (4) coincides with the result of Ref. [48] for both $\lambda = 0$ and $\lambda = \pm 1$ after adjusting for an overall factor of $-\sqrt{N_c}$ due to the difference in conventions. Comparing to Ref. [49] the result coincides for

$\lambda = 0$ (again up to a factor $-\sqrt{N_c}$) but there is an opposite overall sign for $\lambda = \pm 1$ (the relative factor being $+\sqrt{N_c}$), as also explicitly noted in [49]. While such overall signs play no role for the processes involving overlaps of photons and vector quarkonia, the sign is important for tensor quarkonia, since the tensor wave function can be understood as a linear superposition of the vector wave functions; see Eq. (12) below. The computation described in Appendix A takes the LB spinors as a starting point from which we proceed to explicitly compute the photon wave function as well as all the subsequent quarkonia wave functions in a systematic and self-contained fashion.

The explicit expressions for the quarkonia wave functions will be given in the following subsection. Here we want to emphasize that thanks to the $C = +1$ parity of the quarkonium wave function [see Eq. (10) below] and to the $C = -1$ parity of the photon, the amplitude is strictly proportional to the $C = -1$ odderon amplitude $\mathcal{O}(r_\perp, b_\perp)$. In the high-energy limit of eikonal dipole-proton scattering we have [11,12]

$$\mathcal{O}(r_\perp, b_\perp) = -\frac{1}{2iN_c} \text{tr} \langle V(x_\perp)V^\dagger(y_\perp) - V(y_\perp)V^\dagger(x_\perp) \rangle, \quad (5)$$

where $r_\perp$ is the dipole size and $b_\perp$ the impact parameter

$$r_\perp \equiv x_\perp - y_\perp, \qquad b_\perp \equiv \frac{x_\perp + y_\perp}{2}, \quad (6)$$

respectively.[5] $V(x_\perp)$ and $V^\dagger(x_\perp)$ represent Wilson lines at transverse coordinate $x_\perp$ which describe the propagation of the quark and antiquark, respectively, through the A^+ color field of the target proton in covariant gauge; and $\langle \cdots \rangle$

denotes an average over the configurations of that field; see Appendix D for the conventions used in this work.

In Fourier space, the odderon amplitude is given by

$$\mathcal{O}(r_\perp, \Delta_\perp) \equiv \int_{b_\perp} e^{-i\Delta_\perp \cdot b_\perp} \mathcal{O}(r_\perp, b_\perp). \quad (7)$$

The C-invariance of the full amplitude (1) is now easily verified. We can conventionally start by first exchanging the quark-antiquark coordinates $x_\perp \leftrightarrow y_\perp$ so that $r_\perp \to -r_\perp$ in the odderon amplitude. Because of the phases in (2) this needs to be followed by an exchange of quark and antiquark transverse momenta $l_\perp \leftrightarrow l'_\perp - z\Delta_\perp$ and $z \leftrightarrow \bar{z}$. By this transformation only the photon wave function picks up a sign which cancels with the sign in the transformation of the odderon amplitude as $\mathcal{O}(-r_\perp, b_\perp) = -\mathcal{O}(r_\perp, b_\perp)$.

A. Light-cone wave function of C-even quarkonia

The light-cone wave function of the C-even quarkonia, $\Psi^{\mathcal{H}}_{\bar{\lambda},h\bar{h}}$, is modeled by the following covariant ansatz:

$$\Psi^{\mathcal{H}}_{\bar{\lambda},h\bar{h}}(k_\perp, z) \equiv \frac{1}{\sqrt{z\bar{z}}} \bar{u}_h(k)\Gamma^{\mathcal{H}}_{\bar{\lambda}}(k, k')v_{\bar{h}}(k')\phi_{\mathcal{H}}(k_\perp, z). \quad (8)$$

Here $\bar{\lambda}$ is the quarkonium helicity and k ($k' = \Delta_0 - k$) is the quark (antiquark) momentum, with Δ_0 the invariant four momentum of the $c\bar{c}$ pair. $\Gamma^{\mathcal{H}}_{\bar{\lambda}}$ is the appropriate Dirac matrix vertex function for either a scalar ($\mathcal{H} = \mathcal{S}$), axial vector ($\mathcal{H} = \mathcal{A}$), or a tensor ($\mathcal{H} = \mathcal{T}$) quarkonium which we take as[6]

$$\Gamma^{\mathcal{H}}_{\bar{\lambda}}(k, k') = \begin{cases} 1, & \mathcal{H} = \mathcal{S}, \\ i\gamma_5 \not{E}(\bar{\lambda}, \Delta_0), & \mathcal{H} = \mathcal{A}, \\ \frac{1}{2}(\gamma_\mu(k_\nu - k'_\nu) + \gamma_\nu(k_\mu - k'_\mu))E^{\mu\nu}(\bar{\lambda}, \Delta_0), & \mathcal{H} = \mathcal{T}. \end{cases} \quad (9)$$

$\phi_{\mathcal{H}}(k_\perp, z)$ is a nonperturbative scalar function that we model later (see Sec. IV).

The structure of (9) is motivated in part to ensure the correct C-even property of the quarkonia wave function in (8). Namely, by exchanging the quark and the antiquark momenta ($k \leftrightarrow k'$) and helicity ($h \leftrightarrow \bar{h}$) we have

$$\bar{u}_{\bar{h}}(k')\Gamma^{\mathcal{H}}_{\bar{\lambda}}(k', k)v_h(k) = +\bar{u}_h(k)\Gamma^{\mathcal{H}}_{\bar{\lambda}}(k, k')v_{\bar{h}}(k'), \quad (10)$$

which holds thanks to the relation $C(\Gamma^{\mathcal{H}}_{\bar{\lambda}}(k', k))^T C^{-1} = +\Gamma^{\mathcal{H}}_{\bar{\lambda}}(k, k')$ with $C = i\gamma^0\gamma^2$. Furthermore, the $\Gamma^{\mathcal{T}}_{\bar{\lambda}}(k, k')$ vertex is modeled as a coupling to the fermionic energy-momentum tensor; see, e.g., [50–53].

In Eq. (9) the $E(\bar{\lambda}, \Delta_0)$ describe the polarization state of the axial quarkonia. To ensure that the axial vector carries the correct quantum numbers, we require the transversality condition

$$\Delta_0 \cdot E(\bar{\lambda}, \Delta_0) = 0. \quad (11)$$

---

[5]The impact parameter of the dipole-proton collision is actually $\tilde{b}_\perp = zx_\perp + \bar{z}y_\perp = b_\perp - (\frac{1}{2} - z)r_\perp$, and $\tilde{b}_\perp$ is the Fourier conjugate of the transverse momentum transfer $\Delta_\perp$. This is the origin of the "off-forward phase" $-i\delta_\perp \cdot r_\perp$ in Eq. (18).

[6]Our convention is $\gamma^5 \equiv +i\gamma^0\gamma^1\gamma^2\gamma^3$ and $\epsilon^{0123} \equiv +1 = -\epsilon^{+-12}$.

This way, in the $c\bar{c}$ rest frame, $E^\mu(\bar{\lambda}, \Delta_0)$, reduces to its spatial components corresponding to the total spin vector of the $c\bar{c}$ state. Recall that in the light-cone formulation the "−" and ⊥ components of Δ_0 are exactly equal to the corresponding components of the quarkonia four-momentum Δ, but that the "+" components differ: $\Delta^+ = (M_\mathcal{H}^2 + \Delta_\perp^2)/2\Delta^-$ and $\Delta_0^+ = (M_0^2 + \Delta_\perp^2)/2\Delta^-$ with $M_0^2 = \Delta_0^2$ being the invariant mass of the $c\bar{c}$ pair and $M_\mathcal{H}^2 = \Delta^2$ the quarkonia mass. This is because the $c\bar{c}$ pair is allowed to be virtual in the "+" component, conjugate to the light-cone time. Explicitly, we have

$$E^\mu(\bar{\lambda} = \pm 1, \Delta_0) = \left(\frac{\boldsymbol{\epsilon}_\perp^{\bar{\lambda}} \cdot \boldsymbol{\Delta}_\perp}{\Delta^-}, 0, \boldsymbol{\epsilon}_\perp^{\bar{\lambda}} \right),$$

$$E^\mu(\bar{\lambda} = 0, \Delta_0) = \left(\frac{\boldsymbol{\Delta}_\perp^2 - M_0^2}{2M_0\Delta^-}, \frac{\Delta^-}{M_0}, \frac{\boldsymbol{\Delta}_\perp}{M_0} \right)$$
$$= \frac{1}{M_0}\Delta_0^\mu - \frac{M_0}{\Delta^-}n^\mu. \qquad (12)$$

Using Δ instead of Δ_0 has no effect on the $\bar{\lambda} = \pm 1$ components, namely $E^\mu(\bar{\lambda} = \pm 1, \Delta_0) = E^\mu(\bar{\lambda} = \pm 1, \Delta)$. However, the $\bar{\lambda} = 0$ case differs as

$$E^\mu(\bar{\lambda} = 0, \Delta) = \frac{1}{M_\mathcal{A}}\Delta^\mu - \frac{M_\mathcal{A}}{\Delta^-}n^\mu. \qquad (13)$$

We have checked that the projector $i\gamma_5 \not{E}(\bar{\lambda} = 0, \Delta)$ (instead of $i\gamma_5 \not{E}(\bar{\lambda} = 0, \Delta_0)$) leads to incorrect results for the $c\bar{c}$ state as it leaves an admixture with spin different from one. This happens because in the light-cone formulation the rest frames of the quarkonia and of the $c\bar{c}$ partonic state in general move with different velocities, which is a consequence of the difference in their "+" components of the four momenta. The necessary condition for the correct projector, $\Delta_0 \cdot E(\bar{\lambda}, \Delta) = 0$, is fulfilled if and only if $M_0 = M_\mathcal{A}$. In other words, we will assume that the amplitude for the transition from $E^\mu(\bar{\lambda} = 0, \Delta_0)$ to $E^\mu(\bar{\lambda} = 0, \Delta)$ is equal to one. A similar approach was used in Ref. [54]. The underlying principle of parton-hadron duality is also the basis for the successful approach to exclusive ρ^0 electro-production [55,56].

The tensor quarkonia polarizations $E^{\mu\nu}(\bar{\lambda}, \Delta_0)$ can be obtained in terms of $E^\mu(\bar{\lambda}, \Delta_0)$, using Clebsch–Gordan coefficients. We have [50]

$$E^{\mu\nu}(\pm 2, \Delta_0) = E^\mu(\pm 1, \Delta_0)E^\nu(\pm 1, \Delta_0),$$

$$E^{\mu\nu}(\pm 1, \Delta_0) = \frac{1}{\sqrt{2}}(E^\mu(\pm 1, \Delta_0)E^\nu(0, \Delta_0)$$
$$+ E^\mu(0, \Delta_0)E^\nu(\pm 1, \Delta_0)),$$

$$E^{\mu\nu}(0, \Delta_0) = \frac{1}{\sqrt{6}}(E^\mu(+1, \Delta_0)E^\nu(-1, \Delta_0)$$
$$+ E^\mu(-1, \Delta_0)E^\nu(+1, \Delta_0)$$
$$+ 2E^\mu(0, \Delta_0)E^\nu(0, \Delta_0)). \qquad (14)$$

These polarization tensors are traceless, $g_{\mu\nu}E^{\mu\nu}(\bar{\lambda}, \Delta_0) = 0$, and symmetric, $E^{\mu\nu}(\bar{\lambda}, \Delta_0) = E^{\nu\mu}(\bar{\lambda}, \Delta_0)$. We also have transversality conditions, $\Delta_0^\mu E_{\mu\nu}(\bar{\lambda}, \Delta_0) = 0 = \Delta_0^\nu E_{\mu\nu}(\bar{\lambda}, \Delta_0)$, as a consequence of (11). We have checked that Eq. (14) is consistent with the polarization tensors written in [52], up to overall signs.

It is instructive to explicitly compute the quarkonia wave functions in this approach. Using LB spinors [47] we find for the scalar quarkonia

$$\Psi_{h\bar{h}}^\mathcal{S}(\boldsymbol{k}_\perp, z) = \frac{1}{z\bar{z}}[hk_\perp e^{-ih\phi_k}\delta_{h\bar{h}} - m_c(z - \bar{z})\delta_{h,-\bar{h}}]\phi_\mathcal{S}(\boldsymbol{k}_\perp, z). \qquad (15)$$

The helicity structure of the wave function agrees completely with the result in [57]; see (A.18) there. For the axial quarkonia we have

$$\Psi_{+1,h\bar{h}}^\mathcal{A}(\boldsymbol{k}_\perp, z) = -\frac{\sqrt{2}i}{z\bar{z}}[k_\perp e^{i\phi_k}(\bar{z}\delta_{h+}\delta_{\bar{h}-} + z\delta_{h-}\delta_{\bar{h}+})$$
$$+ m_c(z - \bar{z})\delta_{h+}\delta_{\bar{h}+}]\phi_{\mathcal{A},T}(\boldsymbol{k}_\perp, z),$$

$$\Psi_{-1,h\bar{h}}^\mathcal{A}(\boldsymbol{k}_\perp, z) = -\frac{\sqrt{2}i}{z\bar{z}}[k_\perp e^{-i\phi_k}(\bar{z}\delta_{h+}\delta_{\bar{h}-} + z\delta_{h-}\delta_{\bar{h}+})$$
$$- m_c(z - \bar{z})\delta_{h-}\delta_{\bar{h}-}]\phi_{\mathcal{A},T}(\boldsymbol{k}_\perp, z),$$

$$\Psi_{0,h\bar{h}}^\mathcal{A}(\boldsymbol{k}_\perp, z) = -\frac{i}{z\bar{z}}\frac{1}{M_\mathcal{A}}(2\boldsymbol{k}_\perp^2 h\delta_{h,-\bar{h}} + 2m_c k_\perp e^{-ih\phi_k}\delta_{h\bar{h}})$$
$$\times \phi_{\mathcal{A},L}(\boldsymbol{k}_\perp, z), \qquad (16)$$

where $k_\perp e^{\pm i\phi_k} \equiv k^1 \pm ik^2$. At this point we have introduced different scalar functions $\phi_{\mathcal{A},T}(r_\perp, z)$ and $\phi_{\mathcal{A},L}(r_\perp, z)$ for transversely and longitudinally polarized quarkonia.[7] The helicity structure of (16) coincides with the axial part of the Z-boson wave function from Refs. [58,59]. In Ref. [60] the axial quarkonia wave function was computed starting from the quarkonia rest frame followed by a Melosh transformation. The resulting wave functions, their Eqs. (A.7) and (A.9), agree up to an overall normalization constant with (16).

For the tensor quarkonia we obtain the following results

$$\Psi_{+2,h\bar{h}}^\mathcal{T}(\boldsymbol{k}_\perp, z) = -\frac{2}{z\bar{z}}k_\perp e^{i\phi_k}[k_\perp e^{i\phi_k}(z\delta_{h+}\delta_{\bar{h}-} - \bar{z}\delta_{h-}\delta_{\bar{h}+})$$
$$+ m_c\delta_{h+}\delta_{\bar{h}+}]\phi_{\mathcal{T},T2}(\boldsymbol{k}_\perp, z),$$

$$\Psi_{-2,h\bar{h}}^\mathcal{T}(\boldsymbol{k}_\perp, z) = \frac{2}{z\bar{z}}k_\perp e^{-i\phi_k}[k_\perp e^{-i\phi_k}(\bar{z}\delta_{h+}\delta_{\bar{h}-} - z\delta_{h-}\delta_{\bar{h}+})$$
$$+ m_c\delta_{h-}\delta_{\bar{h}-}]\phi_{\mathcal{T},T2}(\boldsymbol{k}_\perp, z),$$

---

[7]For the sake of simplicity, in the case of $\bar{\lambda} = 0$, we have redefined $\phi_{\mathcal{A},L}(\boldsymbol{k}_\perp, z)/M_0 \to \phi_{\mathcal{A},L}(\boldsymbol{k}_\perp, z)/M_\mathcal{A}$, which introduces only subleading effects in the heavy quark limit.

$$\Psi^{\mathcal{T}}_{+1,h\bar{h}}(\mathbf{k}_\perp,z) = \frac{M_{\mathcal{T}}}{z\bar{z}} [-k_\perp e^{i\phi_k}((3z-4z^2)\delta_{h+}\delta_{\bar{h}-}$$
$$+ (3\bar{z}-4\bar{z}^2)\delta_{h-}\delta_{\bar{h}+}) + m_c(z-\bar{z})\delta_{h+}\delta_{\bar{h}+}]$$
$$\times \phi_{\mathcal{T},T}(\mathbf{k}_\perp,z),$$

$$\Psi^{\mathcal{T}}_{-1,h\bar{h}}(\mathbf{k}_\perp,z) = \frac{M_{\mathcal{T}}}{z\bar{z}} [k_\perp e^{-i\phi_k}((3\bar{z}-4\bar{z}^2)\delta_{h+}\delta_{\bar{h}-}$$
$$+ (3z-4z^2)\delta_{h-}\delta_{\bar{h}+}) + m_c(z-\bar{z})\delta_{h-}\delta_{\bar{h}-}]$$
$$\times \phi_{\mathcal{T},T}(\mathbf{k}_\perp,z),$$

$$\Psi^{\mathcal{T}}_{0,h\bar{h}}(\mathbf{k}_\perp,z) = \frac{\sqrt{2}}{\sqrt{3}}\frac{1}{z\bar{z}} [(3\mathbf{k}_\perp^2 + 2m_c^2)(z-\bar{z})\delta_{h,-\bar{h}}$$
$$+ m_c(k_\perp e^{-i\phi_k}\delta_{h+}\delta_{\bar{h}+} - k_\perp e^{i\phi_k}\delta_{h-}\delta_{\bar{h}-})]$$
$$\times \phi_{\mathcal{T},L}(\mathbf{k}_\perp,z). \quad (17)$$

The three different scalar functions $\phi_{\mathcal{T},T2}(\mathbf{k}_\perp,z)$, $\phi_{\mathcal{T},T}(\mathbf{k}_\perp,z)$, and $\phi_{\mathcal{T},L}(\mathbf{k}_\perp,z)$ account for the two possible transverse and longitudinal polarizations of the tensor quarkonia.[8] Comparing to Eq. (13) in Ref. [50], the wave function for $\bar{\lambda}=+2$ polarization agrees with the first line in (17) up to an overall normalization constant. For $\bar{\lambda}=-2$ we find an opposite relative sign between the two terms in square brackets [we agree, though, with the relative sign for $\bar{\lambda}=-2$ in Eq. (B.3) of [50]]. For $\bar{\lambda}=\pm1$ and $\bar{\lambda}=0$ the results agree up to an overall normalization constant.

At this point we comment on the spin-momentum structure of the wave functions in the rest frame. The C parity of a $q\bar{q}$ bound state is $C=(-1)^{L+S}$ and the χ_{cJ} quarkonia with $J=0$, 1, and 2 have been classified by the Particle Data Group as P-waves[9] ($L=1$) [34]. Also, they are spin triplets, $S=1$. Based on our model wave function (8) we therefore explicitly checked that, after replacing the light-cone LB spinors with Dirac spinors ($u_h(k) \to u_s(k)$ and $v_h(k) \to v_s(k)$), the wave functions in the rest frame take their expected nonrelativistic ^3P_J spin-momentum structure. The scalar wave function is proportional to $\xi_{\bar{s}}^\dagger(\boldsymbol{\sigma}\cdot\mathbf{k})\tilde{\xi}_s$, while the axial-vector meson is $\xi_{\bar{s}}^\dagger\boldsymbol{\sigma}\cdot(\mathbf{k}\times\mathbf{E})\tilde{\xi}_s$ [54,57,60,61]. Here ξ_s are the standard two-component Pauli spinors and $\tilde{\xi}_s=i\sigma_2\xi_s^*$. For the tensor wave function we obtain $\xi_{\bar{s}}^\dagger E^{ij}\sigma_i k_j\tilde{\xi}_s$ [62], at leading order in the nonrelativistic limit.

B. Final expressions for the amplitudes

For explicit computations it is convenient to write the reduced amplitude (2) in the following equivalent form; see, e.g., Refs. [17,48,63]

---

[8] In the case $\bar{\lambda}=\pm1$ we have redefined $M_0\phi_{\mathcal{T},T}(\mathbf{k}_\perp,z) \to M_{\mathcal{T}}\phi_{\mathcal{T},T}(\mathbf{k}_\perp,z)$.

[9] For the $J=2$ tensor meson an F-wave component is possible, in principle. Due to the small velocities of the quarks in the rest frame of the meson, this component should be small, to agree with the PDG classification of the χ_{c2} as a P-wave.

$$\mathcal{A}_{\lambda\bar{\lambda}}(\mathbf{r}_\perp,\boldsymbol{\Delta}_\perp) = eq_c \int_z e^{-i\boldsymbol{\delta}_\perp\cdot\mathbf{r}_\perp} \int_{\mathbf{l}_\perp} \frac{e^{i\mathbf{l}_\perp\cdot\mathbf{r}_\perp}}{\mathbf{l}_\perp^2+\varepsilon^2} \int_{\mathbf{l}'_\perp} e^{-i(\mathbf{l}'_\perp - z\boldsymbol{\Delta}_\perp)\cdot\mathbf{r}_\perp}$$
$$\times \phi_{\mathcal{H}}(\mathbf{l}'_\perp - z\boldsymbol{\Delta}_\perp,z)\frac{1}{z\bar{z}}A_{\lambda\bar{\lambda}}(\mathbf{l}_\perp,\mathbf{l}'_\perp - z\boldsymbol{\Delta}_\perp,z),$$
$$(18)$$

where $\boldsymbol{\delta}_\perp = \frac{1}{2}(z-\bar{z})\boldsymbol{\Delta}_\perp = (z-\frac{1}{2})\boldsymbol{\Delta}_\perp$. The helicity sum in (2) is turned into a covariant Dirac trace

$$A_{\lambda\bar{\lambda}}(\mathbf{l}_\perp,\mathbf{l}'_\perp - z\boldsymbol{\Delta}_\perp,z)$$
$$= \frac{1}{(2q^-)^2} \mathrm{tr}[(\not{l}+m_c)\epsilon(\lambda,q)(\not{l}-\not{q}+m_c)$$
$$\times \gamma^-(\not{l}'-\not{\Delta}+m_c)\Gamma_{\bar{\lambda}}^{\mathcal{H}*}(l',\Delta-l')(\not{l}'+m_c)\gamma^-], \quad (19)$$

containing the physical information on the polarization-dependent part of the photon-quarkonia wave function overlap. Together with Eq. (1), Eqs. (18) and (19) comprise the main formulas that will be used below to write the $\gamma^*p\to\mathcal{H}p$ amplitudes in a form suitable for numerical computations. For the explicit evaluation of the traces we have used FeynCalc [64].

We start with the computation of the amplitude for scalar quarkonium. Inserting the first line of (9) into (19) yields

$$A_{\lambda=0}(\mathbf{l}_\perp,\mathbf{l}_{1\perp},z) = -4m_cQz\bar{z}(z-\bar{z}),$$
$$A_{\lambda=\pm1}(\mathbf{l}_\perp,\mathbf{l}_{1\perp},z) = -2m_c[(z-\bar{z})^2(\boldsymbol{\epsilon}_\perp^\lambda\cdot\mathbf{l}_\perp)-(\boldsymbol{\epsilon}_\perp^\lambda\cdot\mathbf{l}_{1\perp})],$$
$$(20)$$

where $\mathbf{l}_{1\perp} \equiv \mathbf{l}'_\perp - z\boldsymbol{\Delta}_\perp$. As a cross check, note that the traces (20) are odd under joint $\mathbf{l}_\perp\to-\mathbf{l}_\perp$, $\mathbf{l}_{1\perp}\to-\mathbf{l}_{1\perp}$ and $z\to\bar{z}$ transformation. In other words, the reduced amplitude $\mathcal{A}_\lambda(\mathbf{r}_\perp,\boldsymbol{\Delta}_\perp)$ in (18) is odd under $\mathbf{r}_\perp\to-\mathbf{r}_\perp$. This is consistent with $\mathcal{O}(\mathbf{r}_\perp,\boldsymbol{\Delta}_\perp)$ being odd under $\mathbf{r}_\perp\to-\mathbf{r}_\perp$ in the full amplitude (1).

We now plug (20) into (18) and Fourier transform to coordinate space. After separating the explicit polarization dependence, the reduced amplitudes are found to be

$$\mathcal{A}_0(\mathbf{r}_\perp,\boldsymbol{\Delta}_\perp) = eq_c \int_z e^{-i\boldsymbol{\delta}_\perp\cdot\mathbf{r}_\perp}\mathcal{A}_L(r_\perp),$$

$$\mathcal{A}_{\lambda=\pm1}(\mathbf{r}_\perp,\boldsymbol{\Delta}_\perp) = eq_c\lambda e^{i\lambda\phi_r} \int_z e^{-i\boldsymbol{\delta}_\perp\cdot\mathbf{r}_\perp}\mathcal{A}_T(r_\perp), \quad (21)$$

where

$$\mathcal{A}_L(r_\perp) \equiv -\frac{2}{\pi}m_cQ(z-\bar{z})K_0(\varepsilon r_\perp)\phi_{\mathcal{S}}(r_\perp,z),$$

$$\mathcal{A}_T(r_\perp) \equiv \frac{i\sqrt{2}}{2\pi}\frac{m_c}{z\bar{z}} \left[(z-\bar{z})^2\varepsilon K_1(\varepsilon r_\perp)\phi_{\mathcal{S}}(r_\perp,z) \right.$$
$$\left. - K_0(\varepsilon r_\perp)\frac{\partial\phi_{\mathcal{S}}}{\partial r_\perp}\right]. \quad (22)$$

In the amplitude (1) we are left with the $r_\perp$ integral and the z integral. We use the Jacobi–Anger expansion to compute the ϕ_r integral and find

$$\langle \mathcal{M}_{\lambda=0} \rangle \equiv q^- \tilde{\mathcal{M}}_{\lambda=0} \equiv q^- \tilde{\mathcal{M}}_L,$$
$$\langle \mathcal{M}_{\lambda=\pm 1} \rangle \equiv q^- \tilde{\mathcal{M}}_{\lambda=\pm 1} \equiv q^- \lambda e^{i\lambda\phi_\Delta} \tilde{\mathcal{M}}_T, \qquad (23)$$

where in the first equality we have separated the flux factor and in the second equality the explicit polarization dependence (together with the overall phase). The remainder consists of two different scalar functions

$$\tilde{\mathcal{M}}_L = 8\pi N_c e q_c \sum_{k=0}^{\infty} (-1)^k \int_z \int_0^{\infty} r_\perp \mathrm{d}r_\perp \mathcal{O}_{2k+1}(r_\perp, \Delta_\perp)$$
$$\times \mathcal{A}_L(r_\perp) \mathrm{sgn}(z - \bar{z}) J_{2k+1}(r_\perp \delta_\perp),$$
$$\tilde{\mathcal{M}}_T = 4\pi i N_c e q_c \sum_{k=0}^{\infty} (-1)^k \int_z \int_0^{\infty} r_\perp \mathrm{d}r_\perp \mathcal{O}_{2k+1}(r_\perp, \Delta_\perp)$$
$$\times \mathcal{A}_T(r_\perp)[J_{2k}(r_\perp \delta_\perp) - J_{2k+2}(r_\perp \delta_\perp)], \qquad (24)$$

which are our main expressions to be used in the numerical computations in Sec. V. The sign function appears due to the definition of $\delta_\perp$ as the modulus of the vector $\boldsymbol{\delta}_\perp$: $\delta_\perp = \frac{1}{2}|z - \bar{z}|\Delta_\perp$.

In the limit $\Delta_\perp \to 0$ the above amplitudes scale as

$$\tilde{\mathcal{M}}_L|_{\Delta_\perp \to 0} \sim \Delta_\perp^2, \qquad \tilde{\mathcal{M}}_T|_{\Delta_\perp \to 0} \sim \Delta_\perp. \qquad (25)$$

The scaling exponents are universal and they do not depend on specific details of the odderon exchange amplitude $\mathcal{O}(r_\perp, b_\perp)$.

The quantities $\mathcal{O}_{2k+1}(r_\perp, \Delta_\perp)$ appearing in Eq. (24) are the azimuthal harmonics of the odderon amplitude,

$$\mathcal{O}_{2k+1}(r_\perp, \Delta_\perp) = 2\pi i (-1)^{k+1} \int_0^{\infty} b_\perp \mathrm{d}b_\perp \mathcal{O}_{2k+1}(r_\perp, b_\perp)$$
$$\times J_{2k+1}(\Delta_\perp b_\perp), \qquad (26)$$

where $\mathcal{O}_{2k+1}(r_\perp, b_\perp)$ is extracted from $\mathcal{O}(r_\perp, b_\perp)$ as its Fourier series coefficients

$$\mathcal{O}(r_\perp, b_\perp) = 2\sum_{k=0}^{\infty} \mathcal{O}_{2k+1}(r_\perp, b_\perp) \cos((2k+1)\phi_{rb}),$$
$$\mathcal{O}_{2k+1}(r_\perp, b_\perp) = \frac{1}{2\pi} \int_0^{2\pi} \mathrm{d}\phi_{rb} \mathcal{O}(r_\perp, b_\perp) \cos((2k+1)\phi_{rb}),$$
$$(27)$$

with $\phi_{rb} = \phi_r - \phi_b$.

The calculation for axial-vector quarkonia follows the same steps as for scalar case. Detailed derivations of the formulas can be found in Appendix B. We end up with three different scalar functions:

$$\tilde{\mathcal{M}}_B = 4\pi i N_c e q_c \sum_{k=0}^{\infty} (-1)^k \int_z \int_0^{\infty} r_\perp \mathrm{d}r_\perp \mathcal{O}_{2k+1}(r_\perp, \Delta_\perp)$$
$$\times \mathcal{A}_B(r_\perp)[J_{2k}(r_\perp \delta_\perp) - J_{2k+2}(r_\perp \delta_\perp)],$$
$$B = TL, LT$$

$$\tilde{\mathcal{M}}_{TT} = 8\pi N_c e q_c \sum_{k=0}^{\infty} (-1)^k \int_z \int_0^{\infty} r_\perp \mathrm{d}r_\perp \mathcal{O}_{2k+1}(r_\perp, \Delta_\perp)$$
$$\times \mathcal{A}_{TT}(r_\perp) \mathrm{sgn}(z - \bar{z}) J_{2k+1}(r_\perp \delta_\perp), \qquad (28)$$

with respective reduced amplitudes

$$\mathcal{A}_{LT}(r_\perp) \equiv \frac{\sqrt{2}}{\pi} Q K_0(\varepsilon r_\perp) \frac{\partial \phi_{\mathcal{A},T}}{\partial r_\perp},$$

$$\mathcal{A}_{TL}(r_\perp) \equiv \frac{\sqrt{2}}{\pi} \frac{1}{z\bar{z}} \frac{1}{M_{\mathcal{A}}} \left[-m_c^2 K_0(\varepsilon r_\perp) \frac{\partial \phi_{\mathcal{A},L}}{\partial r_\perp} \right.$$
$$\left. + \varepsilon K_1(\varepsilon r_\perp) \boldsymbol{\nabla}_\perp^2 \phi_{\mathcal{A},L} \right],$$

$$\mathcal{A}_{TT}(r_\perp) \equiv -\frac{i}{\pi} \frac{z - \bar{z}}{z\bar{z}} \left[\frac{\partial \phi_{\mathcal{A},T}}{\partial r_\perp} \varepsilon K_1(\varepsilon r_\perp) - m_c^2 K_0(\varepsilon r_\perp) \phi_{\mathcal{A},T} \right].$$
$$(29)$$

Here the notation $\tilde{\mathcal{M}}_{TT}$ stands for the amplitude with transition from transversely polarized photon to transversely polarized axial quarkonia. In principle, both the polarization-preserving and polarization-flipping transitions would be possible. However, we find that the polarization-flipping transition vanishes, and so $\tilde{\mathcal{M}}_{TT}$ describes only a polarization-preserving transition. Similar notation is used for other contributing amplitudes. When both the photon and the axial-vector quarkonium are longitudinally polarized, the corresponding amplitude also vanishes; see Appendix B for more details.

In the near forward limit, the axial-vector amplitudes scale as

$$\tilde{\mathcal{M}}_{TL,LT}|_{\Delta_\perp \to 0} \sim \Delta_\perp, \qquad \tilde{\mathcal{M}}_{TT}|_{\Delta_\perp \to 0} \sim \Delta_\perp^2. \quad (30)$$

The procedure is again similar for tensor quarkonia, with detailed steps to be found in Appendix B. The final results for the amplitudes are

$$\tilde{\mathcal{M}}_B = -4\pi N_c e q_c \sum_{k=0}^{\infty} (-1)^k \int_z \int_0^{\infty} r_\perp \mathrm{d}r_\perp$$
$$\times \mathcal{O}_{2k+1}(r_\perp, \Delta_\perp) \mathcal{A}_B(r_\perp)$$
$$\times \mathrm{sgn}(z - \bar{z})[J_{2k+3}(r_\perp \delta_\perp) + J_{2k-1}(r_\perp \delta_\perp)],$$
$$B = LT2, TTf,$$

$$\tilde{\mathcal{M}}_B = 4\pi i N_c e q_c \sum_{k=0}^{\infty} (-1)^k \int_z \int_0^{\infty} r_\perp \mathrm{d}r_\perp \mathcal{O}_{2k+1}(r_\perp, \Delta_\perp)$$
$$\times \mathcal{A}_B(r_\perp)[J_{2k}(r_\perp \delta_\perp) - J_{2k+2}(r_\perp \delta_\perp)],$$
$$B = TT2p, LT, TL,$$

$$\tilde{\mathcal{M}}_B = 8\pi N_c eq_c \sum_{k=0}^{\infty} (-1)^k \int_z \int_0^{\infty} r_\perp dr_\perp \mathcal{O}_{2k+1}(r_\perp, \Delta_\perp)$$

$$\times \mathcal{A}_B(r_\perp) \operatorname{sgn}(z - \bar{z}) J_{2k+1}(r_\perp \delta_\perp), \quad B = TTp, LL,$$

$$\tilde{\mathcal{M}}_{TT2f} = 4\pi i N_c eq_c \sum_{k=0}^{\infty} (-1)^k \int_z \int_0^{\infty} r_\perp dr_\perp \mathcal{O}_{2k+1}(r_\perp, \Delta_\perp)$$

$$\times \mathcal{A}_{TT2f}(r_\perp)[J_{2k+4}(r_\perp \delta_\perp) - J_{2k-2}(r_\perp \delta_\perp)], \quad (31)$$

where

$$\mathcal{A}_{LT2}(r_\perp) \equiv \frac{2}{\pi}(z - \bar{z}) Q K_0(\varepsilon r_\perp)\left(\frac{\partial^2 \phi_{T,T2}}{\partial r_\perp^2} - \frac{1}{r_\perp}\frac{\partial \phi_{T,T2}}{\partial r_\perp}\right),$$

$$\mathcal{A}_{TT2p}(r_\perp) \equiv -\frac{i\sqrt{2}}{\pi}\frac{1}{z\bar{z}}\left((z^2 + \bar{z}^2)\varepsilon K_1(\varepsilon r_\perp)\right.$$

$$\times \left(\frac{\partial^2 \phi_{T,T2}}{\partial r_\perp^2} - \frac{1}{r_\perp}\frac{\partial \phi_{T,T2}}{\partial r_\perp}\right)$$

$$\left. + m_c^2 K_0(\varepsilon r_\perp)\frac{\partial \phi_{T,T2}}{\partial r_\perp}\right),$$

$$\mathcal{A}_{TT2f}(r_\perp) \equiv \frac{i2\sqrt{2}}{\pi}\varepsilon K_1(\varepsilon r_\perp)\left(\frac{\partial^2 \phi_{T,T2}}{\partial r_\perp^2} - \frac{1}{r_\perp}\frac{\partial \phi_{T,T2}}{\partial r_\perp}\right),$$

$$\mathcal{A}_{LT}(r_\perp) \equiv -\frac{i}{\pi} Q M_T (3 - 4(z^2 + \bar{z}^2)) K_0(\varepsilon r_\perp)\frac{\partial \phi_{T,T}}{\partial r_\perp},$$

$$\mathcal{A}_{TTp}(r_\perp) = -\frac{M_T}{\sqrt{2}\pi}\frac{z - \bar{z}}{z\bar{z}}\left[m_c^2 K_0(\varepsilon r_\perp)\phi_{T,T}(r_\perp, z)\right.$$

$$\left. - (z - \bar{z})^2 \varepsilon K_1(\varepsilon r_\perp)\frac{\partial \phi_{T,T}}{\partial r_\perp}\right],$$

$$\mathcal{A}_{TTf}(r_\perp) = -\frac{2\sqrt{2}M_T}{\pi}(z - \bar{z})\varepsilon K_1(\varepsilon r_\perp)\frac{\partial \phi_{T,T}}{\partial r_\perp},$$

$$\mathcal{A}_{LL}(r_\perp) = -\frac{2\sqrt{2}Q}{\sqrt{3}\pi}(z - \bar{z}) K_0(\varepsilon r_\perp)(3\nabla_\perp^2 - 2m_c^2)$$

$$\times \phi_{T,L}(r_\perp, z),$$

$$\mathcal{A}_{TL}(r_\perp) = \frac{i}{\pi\sqrt{3}}\frac{1}{z\bar{z}}\left[\varepsilon K_1(\varepsilon r_\perp)(z - \bar{z})^2(3\nabla_\perp^2 - 2m_c^2)\phi_{T,L}\right.$$

$$\left. - m_c^2 K_0(\varepsilon r_\perp)\frac{\partial \phi_{T,L}}{\partial r_\perp}\right]. \quad (32)$$

In this case the LL-type transition is allowed. Also, both the polarization-preserving and the polarization-flipped contributions are allowed, thus explaining the above used notation: p = preserving, f = flipped.

In the near forward limit, the tensor meson amplitudes scale as

$$\tilde{\mathcal{M}}_{LT2,TTf}|_{\Delta_\perp \to 0} \sim \Delta_\perp^2, \qquad \tilde{\mathcal{M}}_{TT2p,LT,TL}|_{\Delta_\perp \to 0} \sim \Delta_\perp,$$

$$\tilde{\mathcal{M}}_{TTp,LL}|_{\Delta_\perp \to 0} \sim \Delta_\perp^2, \qquad \tilde{\mathcal{M}}_{TT2f}|_{\Delta_\perp \to 0} \sim \Delta_\perp^3. \quad (33)$$

These amplitudes, as well as those for scalar and axial-vector mesons given in Eqs. (25) and (30), vanish for $\Delta_\perp \to 0$ at least as fast as[10]

$$\mathcal{M}_{\lambda\bar{\lambda}}|_{\Delta_\perp \to 0} \sim \Delta_\perp^{|\lambda - \bar{\lambda}|}. \quad (34)$$

Such a rule emerges when the helicity change in the t channel at $t \to 0$ is due to the z component of the angular momentum of the t-channel state. The rule then follows from the conservation of the angular momentum along z. However, the conservation of the z component of the angular momentum provides only a lower limit on the power of $\Delta_\perp$. The amplitude cannot decrease any slower in the forward limit but it can decrease faster, i.e., when the coefficient of the relevant tensor obtained from an expansion of the amplitudes in Δ^i vanishes independently of the "canonical" scaling of this tensor.

C. The $\gamma^* p \to \mathcal{H}p$ cross section

Using the $\tilde{\mathcal{M}}_{\lambda\bar{\lambda}}$ amplitudes obtained in Sec. II B for the process $\gamma^*(q)p(P) \to \mathcal{H}(\Delta)p(P')$, the cross section for longitudinal (L) and transverse (T) photons is given by

$$\frac{d\sigma_L(\gamma^* p \to \mathcal{H}p)}{d|t|} = \frac{1}{16\pi}\sum_{\bar{\lambda}=-J}^{J}|\tilde{\mathcal{M}}_{\lambda=0,\bar{\lambda}}(\gamma^* p \to \mathcal{H}p)|^2,$$

$$\frac{d\sigma_T(\gamma^* p \to \mathcal{H}p)}{d|t|} = \frac{1}{16\pi}\frac{1}{2}\sum_{\lambda=\pm 1}\sum_{\bar{\lambda}=-J}^{J}|\tilde{\mathcal{M}}_{\lambda\bar{\lambda}}(\gamma^* p \to \mathcal{H}p)|^2.$$

$$(35)$$

Inserting the scalar quarkonium amplitudes (23) into (35) gives

$$\frac{d\sigma_L(\gamma^* p \to \mathcal{S}p)}{d|t|} = \frac{1}{16\pi}|\tilde{\mathcal{M}}_L|^2,$$

$$\frac{d\sigma_T(\gamma^* p \to \mathcal{S}p)}{d|t|} = \frac{1}{16\pi}|\tilde{\mathcal{M}}_T|^2, \quad (36)$$

where $\tilde{\mathcal{M}}_B$ ($B = L, T$) are given in Eq. (24). For axial-vector quarkonia we find

$$\frac{d\sigma_L(\gamma^* p \to \mathcal{A}p)}{d|t|} = \frac{1}{8\pi}|\tilde{\mathcal{M}}_{LT}|^2,$$

$$\frac{d\sigma_T(\gamma^* p \to \mathcal{A}p)}{d|t|} = \frac{1}{16\pi}(|\tilde{\mathcal{M}}_{TL}|^2 + |\tilde{\mathcal{M}}_{TT}|^2), \quad (37)$$

with $\tilde{\mathcal{M}}_B$ ($B = LT, TL, TT$) given in (28). We have used (B3) (see Appendix B) to relate $\tilde{\mathcal{M}}_{\lambda\bar{\lambda}}$ to $\tilde{\mathcal{M}}_A$. For the tensor quarkonia, the cross sections are

---

[10]We thank the anonymous referee for drawing our attention to this point.

$$\frac{d\sigma_L(\gamma^* p \to \mathcal{T} p)}{d|t|} = \frac{1}{16\pi}(|\tilde{\mathcal{M}}_{LL}|^2 + 2|\tilde{\mathcal{M}}_{LT}|^2 + 2|\tilde{\mathcal{M}}_{LT2}|^2),$$

$$\frac{d\sigma_T(\gamma^* p \to \mathcal{T} p)}{d|t|} = \frac{1}{16\pi}(|\tilde{\mathcal{M}}_{TL}|^2 + |\tilde{\mathcal{M}}_{TTp}|^2 + |\tilde{\mathcal{M}}_{TTf}|^2$$

$$+ |\tilde{\mathcal{M}}_{TT2p}|^2 + |\tilde{\mathcal{M}}_{TT2f}|^2), \tag{38}$$

with $\tilde{\mathcal{M}}_B$ ($B = LL$, LT, $LT2$, TL, TTp, TTf, $TT2p$, $TT2f$) collected in (31) and the relationship to $\tilde{\mathcal{M}}_{\lambda\bar{\lambda}}$ in (B7).

D. Odderon amplitude and its evolution with x

Here we discuss the odderon amplitude $\mathcal{O}(\boldsymbol{r}_\perp, \boldsymbol{b}_\perp)$ used later in Sec. V for numerical predictions of the cross section for exclusive χ_{cJ} production. The initial $\mathcal{O}(\boldsymbol{r}_\perp, \boldsymbol{b}_\perp)$ at $x_\mathcal{P} = x_0 = 0.01$ is approximated by the matrix element of the C-odd three-gluon operator. This matrix element has been evaluated numerically and tabulated in Ref. [65] using a phenomenological nonperturbative three-quark light-cone wave function [66,67] supplemented by the first correction of perturbative QCD [24]. We refer to these references for further details. Specifically, we use the table for the first azimuthal harmonic $a_1(r_\perp, b_\perp)$ of the $\mathcal{O}(\boldsymbol{r}_\perp, \boldsymbol{b}_\perp)$ defined in Eq. (5) of Ref. [65]. As explained in Appendix D the definition of $\mathcal{O}(\boldsymbol{r}_\perp, \boldsymbol{b}_\perp)$ in [65] is the same as in this work.[11] The first azimuthal moment is defined in [65] through $\mathcal{O}(\boldsymbol{r}_\perp, \boldsymbol{b}_\perp) = \cos(\phi_{rb})a_1(r_\perp, b_\perp) + \cdots$. Thus, from (27) we have the relationship

$$\mathcal{O}_1(r_\perp, b_\perp) = \frac{1}{2}a_1(r_\perp, b_\perp). \tag{39}$$

We do not account for higher-order harmonics such as $\mathcal{O}_3(r_\perp, b_\perp)$ which has been determined to be very small [65] at x_0 and suppressed further by evolution [14,17]. Presently, yet higher Fourier components are unknown; we expect their effects to be well within the current uncertainty of the leading Fourier harmonic.

To determine $\mathcal{O}(\boldsymbol{r}_\perp, \boldsymbol{b}_\perp)$ for $x_\mathcal{P} < x_0$ we solve the impact parameter dependent [68,69] extension of the Balitsky–Kovchegov (BK) equation [with running coupling kernel (rcBK)] to the coupled nonlinear evolution equations for the Pomeron and the odderon derived in Refs. [11,12] and analyzed in Refs. [13–15]. These equations describe the evolution with rapidity $Y = \ln(x_0/x_\mathcal{P})$ of the real and imaginary parts of the dipole S-matrix. For the real part (the Pomeron), we use the initial condition from [70]. The coupled BK equations for the Pomeron-odderon system are solved in the "local approximation" [70,71], where the
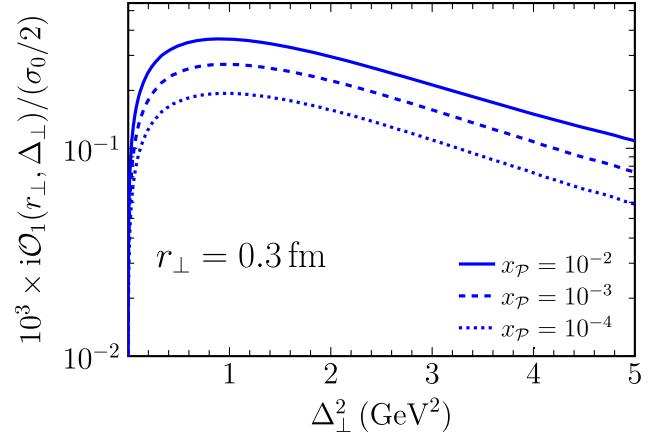

FIG. 2. The first azimuthal harmonic of the odderon amplitude $i\mathcal{O}_1(r_\perp, \Delta_\perp)$ as a function of $\Delta_\perp^2$ for $r_\perp = 0.3$ fm and $\alpha_S = 0.25$. Different line styles correspond to different values of $x_\mathcal{P}$.

impact parameter $\boldsymbol{b}_\perp$ becomes an external parameter. This approximation may be less justified for the odderon than for the Pomeron since the former amplitude peaks at smaller $b_\perp$ [65]. The t dependence of three-gluon exchange is then obtained via Fourier transform, Eq. (7). Technical details of the implementation and additional numerical results can be found in Sec. III of Ref. [17].

Figure 2 shows the first azimuthal harmonic of the odderon amplitude $i\mathcal{O}_1(r_\perp, \Delta_\perp)$ as a function of $\Delta_\perp^2$ for a dipole of size $r_\perp = 0.3$ fm. We have divided by the parameter $\sigma_0/2 = 16.36$ mb $= 42.027$ GeV^{-2} (area of the proton) [70] to compensate for the dimensionality of $i\mathcal{O}_1(r_\perp, \Delta_\perp)$. At $x_\mathcal{P} = 10^{-2}$ this corresponds to the perturbative exchange of three gluons (with negative C parity) while for smaller $x_\mathcal{P}$ the BK resummation has been performed as described above. We note, first of all, the small magnitude of $\mathcal{O}_1(r_\perp, \Delta_\perp) < 10^{-2} \ll 1$, i.e., that scattering of perturbative (small) dipoles via C-odd exchanges is predicted to be very weak. However, we also observe that the C-odd amplitude peaks at fairly large $\Delta_\perp^2 \simeq 1$ GeV^2 and that it decreases by merely a factor of $\sim$2 as $\Delta_\perp^2$ increases further to $\simeq$3 GeV^2. This is a manifestation of the "Landshoff mechanism" [72]; see also [73–75] whereby large t scattering via three-gluon exchange is less likely to break up the proton than scattering via two gluon exchange.[12] In simple terms this is due to the fact that a large momentum transfer can be shared by the exchanged gluons, and so a comparable transverse momentum can be transmitted to up to three partons in the proton, resulting in a smaller increase of their invariant mass than in case of

---

[11]However, our own numerical investigation and private communication with the authors of Ref. [65] revealed that their plots of $\mathcal{O}(\boldsymbol{r}_\perp, \boldsymbol{b}_\perp)$ and their tabulated values actually correspond to minus the function defined in their Eq. (3) and in our Eq. (D11). We therefore reversed the signs of their table entries for $a_1(r_\perp, b_\perp)$.

[12]The proton model light-cone wave function employed here, however, includes a perturbative correction [24] due to the emission of a gluon from one of the valence quarks, or the internal exchange of a gluon, not considered in the quoted papers by Donnachie and Landshoff.

two-gluon exchange. Such a contribution has been illustrated in Fig. 1. The light-cone Fock space amplitudes of the proton are strongly suppressed if the invariant mass of the parton system is far from $\sim N_c \Lambda_{\mathrm{QCD}}$. On the other hand, an amplitude which depends weakly on momentum transfer, in impact parameter space would peak at small $b_\perp$. Amplitudes with negative parity must vanish at $b_\perp = 0$, however, and hence are expected to have small magnitude.

Figure 2 also shows the decrease of the odderon exchange amplitude with $x_{\mathcal{P}}$ by approximately a factor of 2 from $x_{\mathcal{P}} = 10^{-2}$ to $x_{\mathcal{P}} = 10^{-4}$. The initial decrease of the odderon amplitude has been understood to originate from gluon Regge trajectory suppressions in the BJKP equation [11,13,15]. In Appendix E we have checked that by omitting the unitarity corrections, the odderon still decreases but at a smaller rate. Importantly, the sign of the odderon amplitude is preserved by the evolution equation, which is simply a consequence of the fact that its evolution equation is linear in $\mathcal{O}(r_\perp, b_\perp)$.

III. THE PRIMAKOFF CONTRIBUTION

In this section we focus on the Primakoff process, wherein the exclusive $\gamma^* p \to \mathcal{H} p$ production proceeds via photon rather than odderon exchange. Typically, the cross section for a QCD process far exceeds its QED counterparts, and so the latter can be safely neglected. This is, however, not so in case of the odderon because its QCD cross section starts at order α_S^6 and so the QED contribution becomes a competitive background in odderon searches, in particular for low momentum transfer.

We treat the Primakoff process in the high-energy approximation of eikonal scattering, replacing the odderon amplitude $\mathcal{O}(r_\perp, \Delta_\perp)$ in Eq. (1) with [17,33]

$$\mathcal{O}(r_\perp, \Delta_\perp) \to 8\pi i q_c \alpha \sin\left(\frac{\Delta_\perp \cdot r_\perp}{2}\right) \frac{F_1(\Delta_\perp)}{\Delta_\perp^2}, \quad (40)$$

at leading order in the electromagnetic coupling $\alpha = e^2/4\pi$. The amplitude can be written as

$$\langle \mathcal{M}_{\lambda\bar{\lambda}}(\gamma^* p \to \mathcal{H} p) \rangle \equiv -\frac{eF_1(\ell_\perp)}{\ell_\perp^2} n_\mu \mathcal{M}^\mu_{\lambda\bar{\lambda}}(\gamma^*\gamma^* \to \mathcal{H}), \quad (41)$$

where $\mathcal{M}^\mu_{\lambda\bar{\lambda}}(\gamma^*\gamma^* \to \mathcal{H})$ is the $\gamma^*(\lambda, q)\gamma^*(\mu, \ell) \to \mathcal{H}(\bar{\lambda}, \Delta)$ amplitude (in the high-energy limit) that is obtained by inserting (40) into (1). In (41), $\ell \equiv P - P'$ is the momentum transfer from the proton, with $\ell_\perp = \Delta_\perp$ in the dipole frame and $F_1(\ell_\perp)$ is the Dirac charge form factor of the proton with $F_1(0) = 1$; see Appendix D for more detail. Since (40) represents single photon exchange it is more convenient to start from the expression in Eq. (18) for the reduced amplitude and perform the $r_\perp$ integral. This leads to

$$\frac{1}{q^-} n_\mu \mathcal{M}^\mu_{\lambda\bar{\lambda}}(\gamma^*\gamma^* \to \mathcal{H})$$

$$= -8\pi i q_c^2 \alpha N_c \int_z \int_{l_\perp} \left[\frac{A_{\lambda\bar{\lambda}}(l_\perp - \bar{z}\Delta_\perp, l_\perp, z)}{(l_\perp - \bar{z}\Delta_\perp)^2 + \varepsilon^2} \right.$$

$$\left. - \frac{A_{\lambda\bar{\lambda}}(l_\perp + z\Delta_\perp, l_\perp, z)}{(l_\perp + z\Delta_\perp)^2 + \varepsilon^2} \right] \frac{\phi_{\mathcal{H}}(l_\perp, z)}{z\bar{z}}. \quad (42)$$

The term $eF_1(\ell_\perp)/\ell_\perp^2$ in Eq. (41) is understood as a part of the usual Weizsäcker-Williams photon field

$$A^\mu(\ell) = (2\pi)\delta(\ell^-) \frac{1}{\ell_\perp^2} eF_1(\ell_\perp) n^\mu, \quad (43)$$

where n^μ is the light-cone gauge vector.

A. $|t| \to 0$ limit

In the high-energy approximation it is possible to express the $|t| \to 0$ limit of the Primakoff cross section for a C-even quarkonia $\mathcal{H}$ with spin $J \neq 1$ in terms of the two-photon decay width $\Gamma(\mathcal{H} \to \gamma\gamma)$

$$\lim_{|t|\to 0} |t| \frac{d\sigma(\gamma p \to \mathcal{H} p)}{d|t|} = \frac{8\pi\alpha(2J+1)\Gamma(\mathcal{H} \to \gamma\gamma)}{M_{\mathcal{H}}^3}. \quad (44)$$

Equation (44) is a model independent result and not affected by QCD corrections. Hence it represents a stringent constraint on the model predictions and a useful cross check. The key point for obtaining (44) is the relation of the high-energy impact factor for the quarkonia photoproduction to the quarkonia's two-photon decay amplitude. We provide a derivation of (44) in Appendix C. For axial-vector quarkonia, like χ_{c1}, $\Gamma(\mathcal{A} \to \gamma\gamma)$, vanishes and Eq. (44) implies only that $\lim_{|t|\to 0} |t| d\sigma(\gamma p \to \mathcal{A} p)/d|t| = 0$, as is consistent with the Landau–Yang (LY) theorem [76,77], but does not constrain the value of the cross section at $|t| \to 0$. In Appendix C we thus provide a separate and general analysis of the $|t| \to 0$ limit for the axial quarkonia.

In practice, we will use (44) to deduce $\Gamma(\mathcal{H} \to \gamma\gamma)$ from the computation of its left-hand side. This will be required in Sec. IV where we perform a fit of the quarkonia wave functions. Therefore, we now focus on obtaining explicit expressions of the $\gamma^* p \to \mathcal{H} p$ amplitudes in the $|t| \to 0$ (and $Q^2 \to 0$) limit.

Starting with the scalar quarkonia we use (42) and insert the appropriate expressions for the reduced amplitudes $A_{\lambda\bar{\lambda}}(l_\perp, l_{1\perp}, z)$ found in Sec. II B. The relevant reduced amplitude in the $Q^2 \to 0$ limit concerns only the second line of (20). The expression in the square bracket in (42) is conveniently factored as

$$\frac{A_{\lambda=\pm 1}(\boldsymbol{l}_\perp - \bar{z}\boldsymbol{\Delta}_\perp, \boldsymbol{l}_\perp, z)}{(\boldsymbol{l}_\perp - \bar{z}\boldsymbol{\Delta}_\perp)^2 + \varepsilon^2} - \frac{A_{\lambda=\pm 1}(\boldsymbol{l}_\perp + z\boldsymbol{\Delta}_\perp, \boldsymbol{l}_\perp, z)}{(\boldsymbol{l}_\perp + z\boldsymbol{\Delta}_\perp)^2 + \varepsilon^2}$$

$$\to 2m_c \frac{(\boldsymbol{\epsilon}_\perp^\lambda \cdot \boldsymbol{\Delta}_\perp)}{(l_\perp^2 + m_c^2)^2}[l_\perp^2 + (z - \bar{z})^2 m_c^2], \tag{45}$$

where we have set $Q^2 = 0$, performed an expansion around $\Delta_\perp \to 0$ to linear order, as well as the angular average according to $l_\perp^i l_\perp^j \to l_\perp^2 \delta^{ij}/2$. We now insert (45) into (42) and use second line of (23) to extract $\tilde{\mathcal{M}}_T$ as

$$\tilde{\mathcal{M}}_T \to 8\sqrt{2}\pi i q_c^2 \alpha N_c m_c \frac{e F_1(\Delta_\perp)}{\Delta_\perp}$$

$$\times \int_z \int_{l_\perp} \frac{l_\perp^2 + (z - \bar{z})^2 m_c^2}{(l_\perp^2 + m_c^2)^2} \frac{\phi_S(\boldsymbol{l}_\perp, z)}{z\bar{z}}. \tag{46}$$

Performing similar steps for axial quarkonia we find that for the square brackets in (42) the $O(\Delta_\perp)$ contributions vanish for $\bar{\lambda} = 0$ and for $\bar{\lambda} = \pm 1$. A nonvanishing contribution is found for $\bar{\lambda} = \pm 1$ at $O(\Delta_\perp^2)$ leading to

$$\tilde{\mathcal{M}}_{TT} \to -16\pi q_c^2 \alpha N_c e F_1(\Delta_\perp) \int_z \int_{l_\perp} \frac{(z - \bar{z})^2 m_c^2}{(l_\perp^2 + m_c^2)^2} \frac{\phi_A(\boldsymbol{l}_\perp, z)}{z\bar{z}}, \tag{47}$$

while the $\bar{\lambda} = 0$ contribution is $O(\Delta_\perp^3)$. Such a special $\Delta_\perp$ dependence of the axial quarkonia amplitude is explained in Appendix C 2 from general considerations.

For the calculation of the $|t| \to 0$ limit for the tensor quarkonia we also need

$$l_\perp^i l_\perp^j l_\perp^m l_\perp^n \to \frac{1}{8} l_\perp^4 (\delta^{ij}\delta^{mn} + \delta^{im}\delta^{jn} + \delta^{in}\delta^{jm}). \tag{48}$$

Computing for various tensor polarizations $\bar{\lambda}$ we find that $\bar{\lambda} = \pm 1$ does not contribute in the $|t| \to 0$ limit. As for the $\bar{\lambda} = \pm 2$ and $\bar{\lambda} = 0$ cases, we extract the amplitude (31) as

$$\tilde{\mathcal{M}}_{TT2,p} \to 16\sqrt{2}\pi i q_c^2 \alpha N_c \frac{e F_1(\Delta_\perp)}{\Delta_\perp} \int_z \int_{l_\perp} \frac{l_\perp^2}{(l_\perp^2 + m_c^2)^2}$$

$$\times [(z^2 + \bar{z}^2) l_\perp^2 + m_c^2] \frac{\phi_{T,T2}(\boldsymbol{l}_\perp, z)}{z\bar{z}},$$

$$\tilde{\mathcal{M}}_{TT2,f} \to 0,$$

$$\tilde{\mathcal{M}}_{TL} \to -\frac{16}{\sqrt{3}}\pi i q_c^2 \alpha N_c \frac{e F_1(\Delta_\perp)}{\Delta_\perp} \int_z \int_{l_\perp} \frac{m_c^2}{(l_\perp^2 + m_c^2)^2}$$

$$\times \left[l_\perp^2 - 2(z - \bar{z}^2)\left(\frac{3}{2} l_\perp^2 + m_c^2\right)\right] \frac{\phi_{T,L}(\boldsymbol{l}_\perp, z)}{z\bar{z}}. \tag{49}$$

B. Adding the Pauli form factor

In general, the $\gamma^* p \to \mathcal{H} p$ amplitude can be related to the $\gamma^*\gamma^* \to \mathcal{H}$ amplitude by separating out the Dirac current with the Dirac (F_1) and Pauli (F_2) form factors

$$\mathcal{M}_{\lambda\bar{\lambda}}(\gamma^* p \to \mathcal{H} p) = \mathcal{M}_{\lambda\bar{\lambda}}^\mu(\gamma^*\gamma^* \to \mathcal{H})\frac{g_{\mu\nu}}{\ell^2}\bar{u}_{h'}(P')$$

$$\times \left[e F_1(\ell_\perp)\gamma^\nu + i\sigma^{\nu\rho}\ell_\rho \frac{e F_2(\ell_\perp)}{2m_N}\right] u_h(P), \tag{50}$$

where $u_h(P)$ is a proton spinor with helicity h and $\sigma^{\nu\rho} = i[\gamma^\nu, \gamma^\rho]/2$. The dominant contribution of the first term in the high-energy limit is with γ^+, while in the second term the dominant contribution is with σ^{+i}. Thus, we can write in a covariant way

$$\mathcal{M}_{\lambda\bar{\lambda}}(\gamma^* p \to \mathcal{H} p) \approx P_\mu \mathcal{M}_{\lambda\bar{\lambda}}^\mu(\gamma^*\gamma^* \to \mathcal{H})\frac{1}{q \cdot P}\bar{u}_{h'}(P')$$

$$\times \left[\frac{e F_1(\ell_\perp)}{\ell^2}\slashed{q} + i\sigma^{\nu\rho}q_\nu \ell_\rho \frac{e F_2(\ell_\perp)}{2m_N \ell^2}\right]$$

$$\times u_h(P). \tag{51}$$

The above spinor vertices in the high-energy limit become[13]

$$\bar{u}_{h'}(P')\slashed{q}u_h(P) \approx W^2 \delta_{hh'},$$

$$\bar{u}_{h'}(P')i\sigma^{\nu\rho}q_\nu \ell_\rho u_h(P) \approx \ell_\perp h e^{ih\phi_\ell} W^2 \delta_{h,-h'}. \tag{52}$$

With the relation $\langle \mathcal{M}_{\lambda\bar{\lambda}}\rangle = q^- \tilde{\mathcal{M}}_{\lambda\bar{\lambda}} = q^- \mathcal{M}_{\lambda\bar{\lambda}}/W^2$, we have

$$\langle \mathcal{M}_{\lambda\bar{\lambda}}(\gamma^* p \to \mathcal{H} p)\rangle = -n_\mu \mathcal{M}_{\lambda\bar{\lambda}}^\mu(\gamma^*\gamma^* \to \mathcal{H})\left[\frac{e F_1(\ell_\perp)}{\ell_\perp^2}\delta_{hh'}\right.$$

$$\left. + \frac{e F_2(\ell_\perp)}{\ell_\perp^2}\frac{\ell_\perp}{2m_N}h e^{ih\phi_\ell}\delta_{h,-h'}\right], \tag{53}$$

where the first term reproduces (41). Thanks to the difference in the helicity structure in the high-energy limit there is no interference between the F_1 and F_2 contributions in (53). For the same reason there is no intereference of the F_2 term with the odderon exchange amplitude. The addition of F_2 to the Primakoff cross section therefore amounts to a simple replacement

$$F_1^2(\ell_\perp) \to F_1^2(\ell_\perp) + \frac{\ell_\perp^2}{4m_N^2}F_2^2(\ell_\perp). \tag{54}$$

---

[13]The calculation steps are very similar to the one performed in Appendix A and also available in [47].

Thanks to the additional $\ell_\perp$ dependence, the F_2 contribution is negligible at $|t| = \ell_\perp^2 \to 0$ but in practice becomes up to about 50% correction at finite $|t|$ [78].

IV. BOOSTED GAUSSIAN MODEL FOR THE χ_{cJ} WAVE FUNCTIONS

In this section we perform a fit of the scalar part of the C-even quarkonia wave function $\phi_{\mathcal{H},i}(\boldsymbol{k}_\perp, z)$. We adopt a Boosted Gaussian ansatz [79] originally written in coordinate space as

$$\phi_{\mathcal{H},B}(r_\perp, z) = \mathcal{N}_{\mathcal{H},B} z\bar{z} \exp\left(-\frac{m_c^2 \mathcal{R}_{\mathcal{H}}^2}{8z\bar{z}} - \frac{2z\bar{z}r_\perp^2}{\mathcal{R}_{\mathcal{H}}^2} + \frac{1}{2} m_c^2 \mathcal{R}_{\mathcal{H}}^2 \right),$$
(55)

where $\mathcal{R}_{\mathcal{H}}$ is the radii parameter and $\mathcal{N}_{\mathcal{H},i}$ are normalization parameters for different quarkonia species and polarizations that are to be determined below. For $\mathcal{H} = \mathcal{S}$ we have only one normalization, $\mathcal{N}_{\mathcal{S}}$, for $\mathcal{H} = \mathcal{A}$, we have $B = T, L$, denoting transverse and longitudinal polarizations. For $\mathcal{H} = \mathcal{T}$, the index B spans over $B = T2, T, L$. The wave function is normalized as

$$1 = N_c \sum_{h\bar{h}} \int_z \int_{\boldsymbol{r}_\perp} |\Psi_{\bar{\lambda},h\bar{h}}^{\mathcal{H}}(\boldsymbol{r}_\perp, z)|^2.$$
(56)

In practice, we convert (56) to momentum space and express the helicity sum as a Dirac trace as

$$1 = N_c \int_{\boldsymbol{k}_\perp} \int_z \frac{1}{z\bar{z}} \mathrm{tr}[(\slashed{k} - m_c)\gamma^0 \Gamma_{\bar{\lambda}}^{\mathcal{H},\dagger}(k, k')$$
$$\times \gamma^0 (\slashed{k} + m_c) \Gamma_{\bar{\lambda}}^{\mathcal{H}}(k, k')] |\phi_{\mathcal{H},B}(\boldsymbol{k}_\perp, z)|^2.$$
(57)

To constrain the parameters $\mathcal{R}_{\mathcal{H}}$ and $\mathcal{N}_{\mathcal{H},i}$, we use (57) and the $\mathcal{H} \to \gamma\gamma$ decay width for χ_{c0} and χ_{c2}. The $\chi_{c1} \to \gamma\gamma$

decay is forbidden due to the LY theorem. In this case our assumption is that the $\mathcal{R}$ parameter of χ_{c1} is equal to that for χ_{c2}.

The decay rate for $\mathcal{H} = \mathcal{S}$, $\mathcal{T}$ can be obtained from the correspondence in Eq. (44). For scalar quarkonia we first insert the amplitude (46) into (36) to find the $|t| \to 0$ limit of the cross section. We then extract the decay rate via (44) as

$$\Gamma(\mathcal{S} \to \gamma\gamma) = \frac{\pi\alpha^2}{4} M_{\mathcal{S}}^3 F_{\mathcal{S}}^2,$$
$$F_{\mathcal{S}} \equiv 4q_c^2 m_c N_c \int_z \int_{\boldsymbol{k}_\perp} \frac{\boldsymbol{k}_\perp^2 + (z-\bar{z})^2 m_c^2}{(\boldsymbol{k}_\perp^2 + m_c^2)^2} \frac{\phi_{\mathcal{S}}(\boldsymbol{k}_\perp, z)}{z\bar{z}},$$
(58)

which agrees perfectly with Eq. (13) in Ref. [80] after adjusting the conventions. We have additionally confirmed that in the NRQCD limit (58) agrees with the known result in [81] (see Appendix C).

For the actual fit, the LO result in (58) is supplemented by the NLO QCD corrections [81,82]. This amounts to a replacement:

$$\Gamma(\mathcal{S} \to \gamma\gamma) \to \left(1 + \frac{\alpha_S}{\pi}\left(\frac{\pi^2}{3} - \frac{28}{9} \right) \right) \Gamma(\mathcal{S} \to \gamma\gamma)$$
$$\approx (1 + 0.06\alpha_S) \Gamma(\mathcal{S} \to \gamma\gamma).$$
(59)

For the experimental value of $\chi_{c0} \to \gamma\gamma$ decay width we use the most recent PDG value: $\Gamma(\chi_{c0} \to \gamma\gamma) = 2.203 \times 10^{-6}$ GeV [34]. Using $m_c = 1.4$ GeV and $M_{\chi_{c0}} = 3.414$ GeV and $\alpha_S(2m_c) \approx 0.25$, we determine $\mathcal{N}_{\chi_{c0}} = 1.148$ and $\mathcal{R}_{\chi_{c0}} = 1.539$ GeV^{-1}. As expected, the radius parameter $\mathcal{R}$ of the χ_{c0} is similar to that of the J/ψ [79].

For $\mathcal{T}$ we insert the amplitude (49) into (38) and extract the decay rate via (44) as

$$\Gamma(\mathcal{T} \to \gamma\gamma) = \frac{\pi\alpha^2}{20} M_{\mathcal{T}}^3 (F_{\mathcal{T},L}^2 + F_{\mathcal{T},T2}^2),$$
$$F_{\mathcal{T},L} = \frac{4\sqrt{2}}{\sqrt{3}} q_c^2 N_c \int_z \int_{\boldsymbol{k}_\perp} \frac{m_c^2 [\boldsymbol{k}_\perp^2 - 2(z-\bar{z})^2(\frac{3}{2}\boldsymbol{k}_\perp^2 + m_c^2)]}{(\boldsymbol{k}_\perp^2 + m_c^2)^2} \frac{\phi_{\mathcal{T},L}(\boldsymbol{k}_\perp, z)}{z\bar{z}},$$
$$F_{\mathcal{T},T2} = 8q_c^2 N_c \int_z \int_{\boldsymbol{k}_\perp} \frac{\boldsymbol{k}_\perp^2 [(z^2 + \bar{z}^2)\boldsymbol{k}_\perp^2 + m_c^2]}{(\boldsymbol{k}_\perp^2 + m_c^2)^2} \frac{\phi_{\mathcal{T},T2}(\boldsymbol{k}_\perp, z)}{z\bar{z}},$$
(60)

where $F_{\mathcal{T},L}$ ($F_{\mathcal{T},T2}$) originates from the $\bar{\lambda} = 0$ ($\bar{\lambda} = \pm 2$) polarizations. We find only a partial agreement of our result (60) and Eqs. (22)–(24) of [80]. The third line of (60) can be brought in agreement with Eq. (24) in [80] after appropriate adjustments in conventions and also after a judicious identification of $M_{\mathcal{T}}$ with the pair invariant mass M_0. However, the square brackets of the second line in (60)

contain a term $\boldsymbol{k}_\perp^2$ while in (23) of [80] they rather have $-m_c^2$. Using (60) in the NRQCD limit we find the $\bar{\lambda} = 0$ contribution vanishes with the $\bar{\lambda} = \pm 2$ contribution saturating the NRQCD limit completely and in accordance with the known result [81]. Taking the NRQCD limit of (22)–(24) in [80] gives an incorrect result as it leads to a finite contribution from the $\bar{\lambda} = 0$ polarization.

The QCD corrections [81,82] turn out to be sizeable in this particular channel [81,82]

$$\Gamma(\mathcal{T} \to \gamma\gamma) \to \left(1 - \frac{16\alpha_S}{3\pi}\right)\Gamma(\mathcal{T} \to \gamma\gamma)$$

$$\approx (1 - 1.7\alpha_S)\Gamma(\mathcal{T} \to \gamma\gamma). \quad (61)$$

Using $M_{\chi_{c2}} = 3.556$ GeV and the PDG value $\Gamma(\chi_{c2} \to \gamma\gamma) = 5.614 \times 10^{-7}$ GeV [34], we find $\mathcal{N}_{\chi_{c2},T2} = 0.609$ GeV$^{-1} = \mathcal{N}_{\chi_{c2},L}$, $\mathcal{N}_{\chi_{c2},T} = 0.592$ GeV^{-1} and $\mathcal{R}_{\chi_{c2}} = 1.482$ GeV^{-1}. In these numerical estimates we used $\alpha_S = 0.25$ in the NLO correction factors.

Finally, for χ_{c1} we assume $\mathcal{R}_{\chi_{c1}} = \mathcal{R}_{\chi_{c2}}$, allowing us to fix the parameters $\mathcal{N}_{\chi_{c1},T,L}$ via normalization. We find $\mathcal{N}_{\chi_{c1},T} = 1.388$ and $\mathcal{N}_{\chi_{c1},L} = 1.401$.

From the above fits we may compute charge radii of the χ_{cJ} states via the following formula [83]:

$$\langle r_c^2 \rangle = N_c \sum_{h\bar{h}} \int_z \int_{\boldsymbol{r}_\perp} (A_{\bar{\lambda}}^{\mathcal{H}}\bar{z}^2\boldsymbol{r}_\perp^2)|\Psi_{\bar{\lambda},h\bar{h}}^{\mathcal{H}}(\boldsymbol{r}_\perp, z)|^2. \quad (62)$$

$(A_{\bar{\lambda}}^{\mathcal{H}})^{-1}$ denotes the expectation value of $\boldsymbol{r}_\perp^2/r^2 = \sin^2\theta$ in the state

$$|J, \bar{\lambda}\rangle = \sum_{m,m_s} C(J, \bar{\lambda}|L, m; S, m_s)|L, m\rangle|S, m_s\rangle, \quad (63)$$

where $C(J, \bar{\lambda}|L, m; S, m_s)$ denotes the Clebsch–Gordan coefficient for $L = S = 1$. This gives $A_0^{\chi_{c0}} = 3/2$, $A_0^{\chi_{c1}} = 5/4$, $A_1^{\chi_{c1}} = 5/3$, $A_0^{\chi_{c2}} = 15/8$, $A_1^{\chi_{c2}} = 5/3$, and $A_2^{\chi_{c2}} = 5/4$. For χ_{c0} we then find $\sqrt{\langle r_c^2 \rangle} = 0.270$ fm, which is close to the value obtained in Ref. [83] from potential models. For χ_{c1} we find $\sqrt{\langle r_c^2 \rangle} = 0.277$ fm for $\bar{\lambda} = \pm 1$, while $\sqrt{\langle r_c^2 \rangle} = 0.236$ fm was obtained for $\bar{\lambda} = 0$. For χ_{c2} we have $\sqrt{\langle r_c^2 \rangle} = 0.263$ fm for $\bar{\lambda} = \pm 2$, $\sqrt{\langle r_c^2 \rangle} = 0.262$ fm for $\bar{\lambda} = \pm 1$, and $\sqrt{\langle r_c^2 \rangle} = 0.237$ fm for $\bar{\lambda} = 0$. Thus, all charge radii are of comparable magnitude and less than 0.3 fm, which appears reasonable.

V. NUMERICAL RESULTS

In this section we will first show numerical results for the $\gamma^* p \to \chi_{cJ} p$ cross section based on the formulas in Secs. II B and III, for EIC kinematics. Using the $\gamma^* p \to \chi_{cJ} p$ cross sections, we will also compute the electroproduction cross section $e(k)p(P) \to \chi_{cJ}(\Delta)e(k')p(P')$ through the standard formula [84–87]

$$\frac{d\sigma_{ep}}{dx_{\mathcal{P}}dQ^2 d|t|} = \frac{\alpha}{2\pi Q^2 x_{\mathcal{P}}}\left\{2(1-y)\frac{d\sigma_L}{d|t|} + \left(1 + (1-y)^2 - 2(1-y)\frac{Q_{\min}^2}{Q^2}\right)\frac{d\sigma_T}{d|t|}\right\}, \quad (64)$$

where $Q_{\min}^2 = m_e^2 y^2/(1-y)$ accounts for projectile mass corrections, with m_e being the electron mass. y is the inelasticity, given by

$$y \equiv \frac{q \cdot P}{k \cdot P} = \frac{W^2 + Q^2 - m_N^2}{S - m_N^2}, \quad (65)$$

where $S \equiv (k + P)^2$ is the ep collision energy, $W^2 \equiv (q + P)^2$ is the $\gamma^* p$ collision energy, and m_N is the proton mass. Recall that the odderon amplitude evolves with Pomeron-$x_{\mathcal{P}}$, which is related to the conventional Bjorken-x variable $x_B = Q^2/(2q \cdot P) = Q^2/(W^2 + Q^2 - m_N^2)$ via

$$x_{\mathcal{P}} \equiv \frac{x_B}{\beta}, \qquad \beta \equiv \frac{Q^2}{2q \cdot \ell} = \frac{Q^2}{Q^2 + M_{\mathcal{H}}^2 + |t|}. \quad (66)$$

In the numerical computations, we augment the Primakoff cross section by taking into account the Pauli form factor F_2 as explained in Sec. III B. For χ_{c0} and χ_{c2} we take into account the available QCD corrections to the Primakoff cross section via (44). The total cross section is based on taking the coherent sum of the Primakoff and the odderon exchange amplitudes in which case their relative

sign becomes crucial. Our careful analysis in Appendix D reveals that the *Primakoff and odderon amplitudes are in phase*, that is, *they interfere constructively* for each value of the odderon evolution parameter $x_{\mathcal{P}}$, as we have also explained in Sec. II D. The contribution of F_2 does not interfere with the coherent sum of the odderon and Primakoff amplitudes. The interference between the QCD correction to the Primakoff amplitude (available for $\chi_{c0,2}$) and the odderon exchange is determined through the relative phase of the odderon and the Primakoff amplitude at tree level. For the odderon component we use the solutions of the rcBK evolution, keeping only the $k = 0$ harmonic of the Fourier series (27), as explained in Sec. II D. For the Primakoff component we use the recent fits of F_1 and F_2 from [78]. Our standard choice for the QCD coupling α_S is $\alpha_S(2m_c) \approx 0.25$ unless stated otherwise.

We start with the numerical results for the $\gamma^* p \to \chi_{cJ} p$ cross sections shown in Fig. 3 as functions of $|t|$, for different values of $x_{\mathcal{P}}$. We have set $Q^2 = 0.01$ GeV^2. Since Q^2 is low, we focus on the transverse cross section $d\sigma_T/d|t|$. At small $|t|$ the cross section is, of course, dominated by the Primakoff process (photon exchange). However, we note that our predictions for the Primakoff
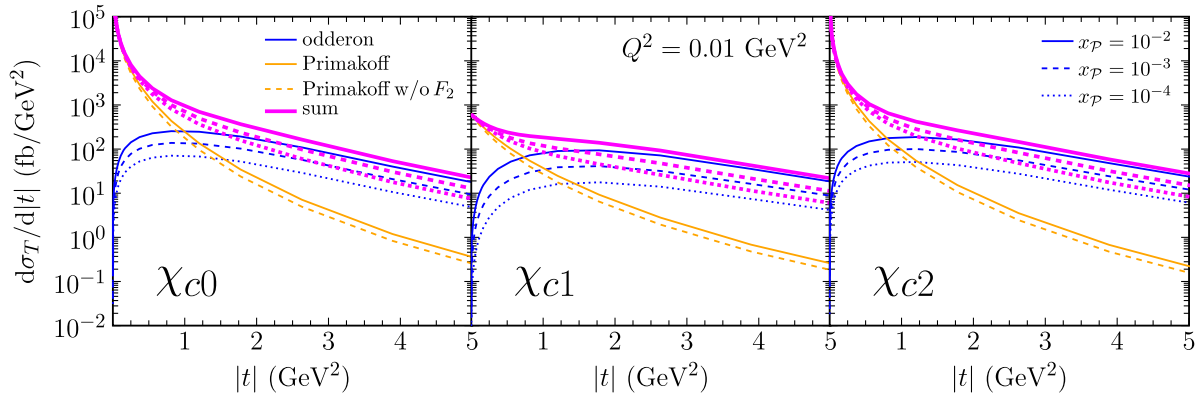
FIG. 3. The $\gamma^* p \to \chi_{cJ} p$ cross sections as functions of $|t|$ for the transverse photon. The label "sum" stands for the coherent sum of the odderon and the Primakoff contributions. We have set $Q^2 = 0.01$ GeV^2. Different line styles in the odderon and the summed cross section correspond to different values of $x_{\mathcal{P}}$. The comparison of the Primakoff contribution with the full and dashed orange lines shows the impact of F_2.

cross sections are substantially lower than those shown in Fig. 4(c) of Ref. [88]. This emphasizes the importance of the constraint (44) from the two photon decay rate.

The QCD odderon exchange amplitude reaches a comparable magnitude at $|t| \approx 1$ GeV^2, depending on $x_{\mathcal{P}}$ and J. The lowest crossover from the Primakoff dominated to the odderon dominated regime at $|t| < 1$ GeV^2 is seen for χ_{c1} and χ_{c2} where the Primakoff-like background is lower than for χ_{c0}. In the regime of $|t|$ where the individual Primakoff and odderon cross sections are of similar magnitude, thanks to their constructive interference, the coherently summed cross section is four times greater than the Primakoff cross section alone. At high-momentum transfer odderon exchange dominates due to its slower fall off with $|t|$.

For Fig. 4 we have integrated $d\sigma_T/d|t|$ over the range $0.5 < |t| < 1.5$ GeV^2 as appropriate for the EIC design detector [44]. We show the result as a function of W. As a consequence of small-x evolution, the odderon cross section drops with increasing W. As the Primakoff cross section is constant, at the lower end of W the coherent sum is about five times greater than the Primakoff component

alone. Interestingly, σ_T displays a negative slope due to the decreasing odderon amplitude towards smaller x.

We find that the decrease of the odderon cross section with W is driven mostly by the nonlinear corrections in the unitarized evolution for the odderon. In Appendix E (see Fig. 9, right) we have computed σ_T based on linear evolution of the BKP odderon and found a slower decrease with W as anticipated from the asymptotics of the BLV solution with an intercept equal to one [9].

We also calculate the differential $ep \to \chi_{cJ} ep$ cross section for top EIC energy, $\sqrt{S} = 140$ GeV, and use the following kinematic cuts: $0.01 < y < 0.95$ [44], $x_{\mathcal{P}} < 0.01$, and $Q^2_{\min} < Q^2 < (2 \times 3.5 \text{ GeV})^2$. The resulting $|t|$ dependence of the cross section is shown in Fig. 5. With these cuts the crossover from photon to odderon exchange occurs at about $|t| \approx 1$ GeV^2 where the total cross section is several times greater than the Primakoff process alone.

The total χ_{cJ} cross sections are shown in Fig. 6. They have been integrated over $|t|$ over the range 0.5 GeV$^2 < |t| < 1.5$ GeV^2 where according to Fig. 5 the odderon
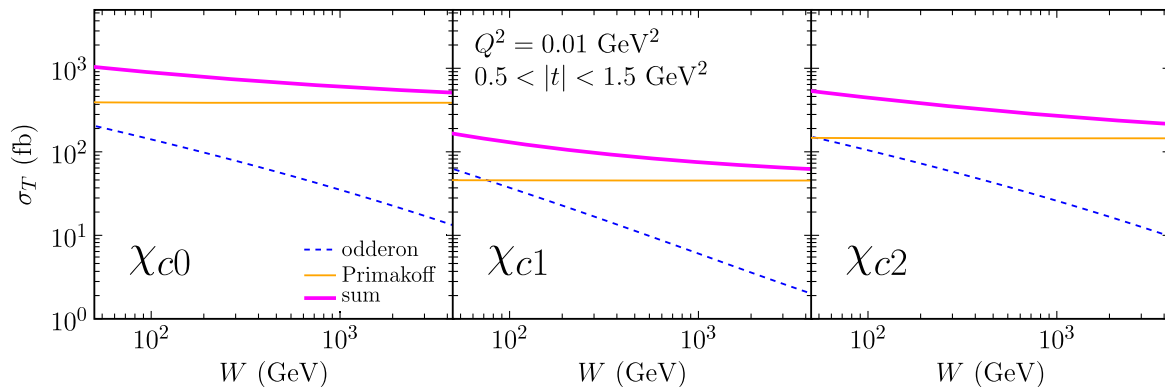

FIG. 4. The $\gamma^* p \to \chi_{cJ} p$ cross sections as functions of W for the transverse photon. The label "sum" stands for the coherent sum of the odderon and Primakoff contributions. We have set $Q^2 = 0.01$ GeV^2 and integrated in $|t|$ over $0.5 < |t| < 1.5$ GeV^2.
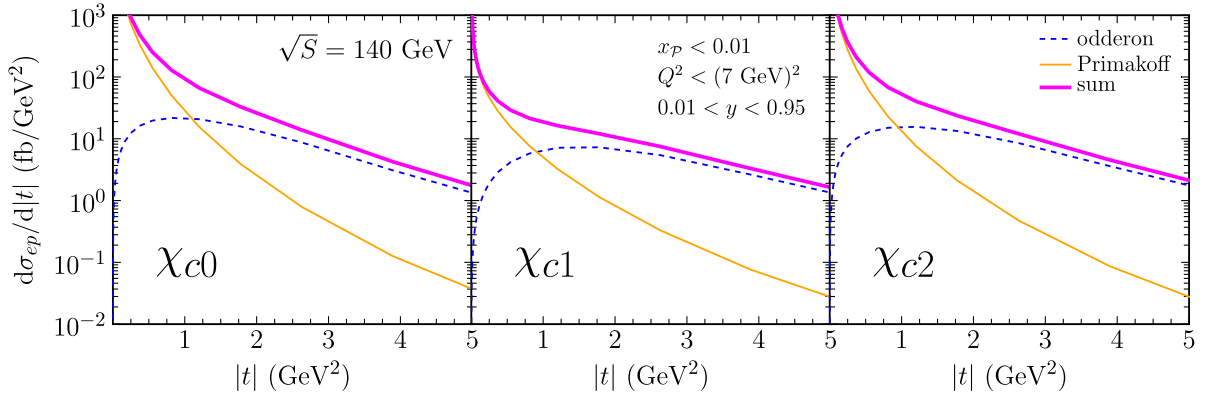
FIG. 5.　The $ep \to \chi_{cJ} ep$ ($J = 0, 1, 2$) cross sections as functions of $|t|$ at the top EIC energy of $\sqrt{S} = 140$ GeV.

contribution is appreciable. Both the photon and odderon exchange contributions level off towards top EIC energy since our kinematic cuts are energy independent, and neither exchange involves a positive intercept.

χ_{c1} has the highest branching ratio $\mathrm{BR}(\chi_{c1} \to J/\psi\gamma) = 34.3\%$ [34]. As an example, let us estimate the total number of χ_{c1}'s per month at the EIC. From Fig. 6 the total cross section is about $\sigma_{ep} \approx 20$ fb at $\sqrt{S} = 140$ GeV. Multiplying by the expected luminosity at the EIC ($L = 10^{34}$ cm^{-2} s$^{-1} = 10^{-5}$ fb^{-1} s^{-1}) gives about 2×10^{-4} events/second or ≈ 518 events/month. After taking into account $\mathrm{BR}(\chi_{c1} \to J/\psi\gamma)$ results in about 177 events/month. J/ψ's are detected through the $J/\psi \to e^+e^-$ or $\to \mu^+\mu^-$ decays, and the combined corresponding branching ratio is about $\mathrm{BR}(J/\psi \to \ell^+\ell^-) = 12\%$, after which we end up with about 21 events/month.

In the final Fig. 7, we summarize the expected number of exclusive χ_{cJ} events per month, $N_{\chi_{cJ}}$, at the EIC design luminosity for two ranges of momentum transfer $|t|$. The result is obtained according to:

$$N_{\chi_{cJ}} = L \times \sigma_{ep}(ep \to \chi_{cJ} ep) \times \mathrm{BR}(\chi_{cJ} \to J/\psi\gamma)$$
$$\times \mathrm{BR}(J/\psi \to \ell^+\ell^-). \qquad (67)$$

The most statistics is expected for χ_{c1} and χ_{c2} tensor quarkonia with about a factor of 2–3 excess events over the Primakoff process in the interval 0.5 GeV$^2 < |t| < 1.5$ GeV^2. The large χ_{c0} cross section in Fig. 6 is compensated by a small branching ratio $\mathrm{BR}(\chi_{c0} \to J/\psi\gamma) = 1.4\%$ [34].

The presented estimates of χ_{cJ} production cross sections carry some theoretical uncertainties. For the photon exchange contribution they are smaller than for the odderon exchange. The coupling of the photon to the proton is well constrained experimentally [78], and so the main sources of uncertainty are the $\gamma^*\gamma^* \to \chi_{cJ}$ amplitudes. They depend on the details of the quarkonia wave functions and are sensitive to unknown higher-order QCD corrections. For χ_{c0} and χ_{c2} the differential cross section $d\sigma/d|t|$ for the Primakoff process obeys a stringent constraint at small $|t| \ll 1$ GeV^2 imposed by Eq. (44) that holds at all orders in QCD. Hence, for these charmonia the uncertainties mentioned above affect mostly the details of the t-shape of $d\sigma/d|t|$. They are expected to be small as the χ_{cJ} wave functions are probed mostly at short distances $\sim 1/m_c$, where they are well constrained by the $\gamma\gamma$ decay width. The value of the coupling $\alpha_S(2m_c) \simeq 0.25$ is not large and the $t \to 0$ limit of the QCD corrections is known, so the
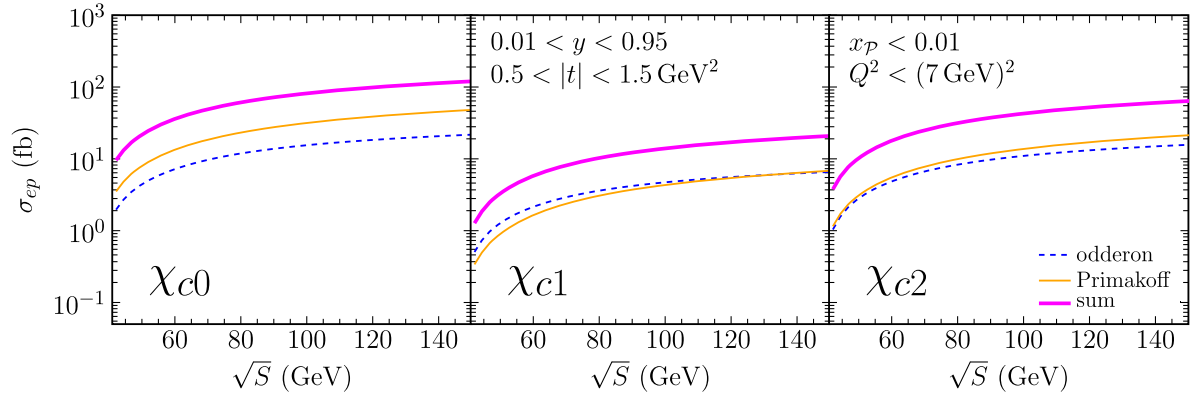

FIG. 6.　Total electroproduction cross section of the χ_{cJ} quarkonia as a function of the ep center of mass energy $\sqrt{S}$. Kinematic cuts are explained in the text.
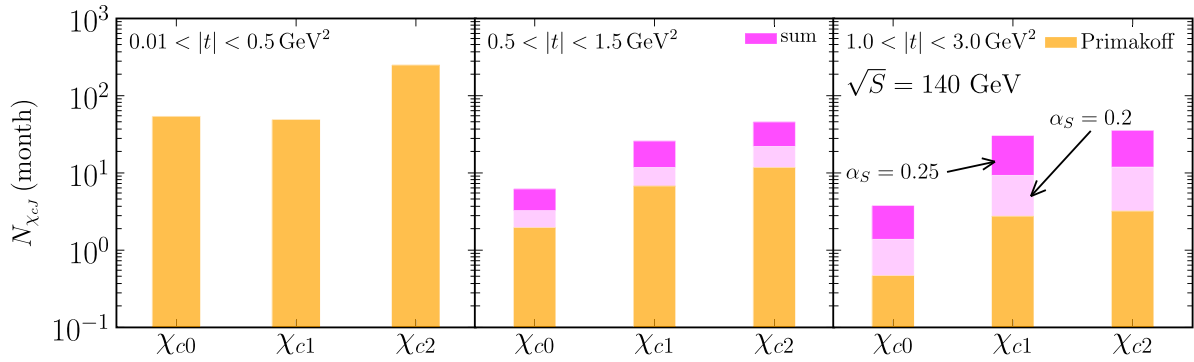
FIG. 7. A summary of expected Primakoff (orange) vs total (magenta) number of exclusive $\chi_{cJ} \to J/\psi\gamma \to l^+l^-\gamma$ events per month at the top EIC energy of $\sqrt{S} = 140$ GeV for three different $|t|$ cuts. The remaining kinematic cuts are the same as in Fig. 6. The two different bins for the total number of events correspond to $\alpha_S = 0.25$ and $\alpha_S = 0.2$, respectively.

uncertainties from QCD corrections at $t \neq 0$ should be small as well. For χ_{c1} the theoretical uncertainty of the Primakoff cross section is larger than for χ_{c0} and χ_{c2}, as the constraint (44) cannot be imposed due to the LY theorem and, in consequence, the vanishing $\gamma\gamma$ decay width of χ_{c1}. In this case measurements of the differential cross sections $d\sigma/d|t|$ for $|t| \ll 1$ GeV^2 where the photon exchange dominates should greatly reduce the uncertainty associated with this contribution at $|t| \sim 1$ GeV^2, where we expect to isolate a significant odderon signal.

In the odderon exchange, in addition to uncertainties from unknown details of the quarkonia wave function and from higher-order QCD corrections, there are uncertainties associated with the model for the proton wave function, and from the value of α_S. The model of the proton employed here obeys general constraints coming from the measurements of the proton size, exclusive J/ψ production of the proton [33] and open charm electroproduction at Hadron–Electron Ring Accelerator (HERA) [65]. Those constraints, however, originate from measurements in the C-even sector, and the emerging C-odd correlators have never been probed experimentally. Furthermore, the perturbative odderon is strongly sensitive to the numerical value of α_S, the amplitude being $O(\alpha_S^3)$ at the lowest order. To quantify the uncertainty in the value of α_S we take an interval $0.2 < \alpha_S < 0.25$. The lower value $\alpha_S = 0.2$ comes from a fit of the proton and C-even exchange models to open charm electroproduction at HERA [65]. Therein the average value of the hard scale $\mu = \sqrt{Q^2 + 4m_c^2}$ is about 5 GeV, so the obtained value $\alpha_S = 0.2$ is fully consistent with the running of $\alpha_S(\mu)$. In our case the bulk of exclusive χ_{cJ} production in ep collisions occurs at small photon virtualities and moderate $|t|$, and so $\alpha_S(2m_c) \approx 0.25$ is more appropriate. The range $0.2 < \alpha_S < 0.25$ results in an uncertainty about a factor of 2.5 between the minimal and maximal values of the odderon amplitude, when NLO effects in the proton wave function are included.

For the combined Primakoff and odderon contributions, the α_S-induced uncertainty is negligible for $|t| \ll 1$ GeV^2,

where the Primakoff process dominates. This uncertainty is about a factor of 2 when Primakoff and odderon (with $\alpha_S = 0.25$) amplitudes are close to each other, and up to a factor of about 6 when the odderon strongly dominates over the Primakoff channel. Since the uncertainty coming from α_S is sizeable, we assume that it is the dominant uncertainty for the odderon exchange and take it as our estimate of the theoretical uncertainty. We consider the choice of $\alpha_S = 0.25$ to be realistic, as the scale $2m_c$ is already fairly high. Another choice is $\mu = m_c$, leading to $\alpha_S \approx 0.35$, as obtained for exclusive J/ψ photoproduction using the same model for the proton at leading order [33]. Thus, we consider the lower value of $\alpha_S = 0.2$ to be a conservative choice.

VI. SUMMARY AND CONCLUSIONS

In this paper we have derived amplitudes for exclusive scalar, axial-vector, and tensor quarkonium production, Eqs. (22), (24), (28), (29), (31), and (32), respectively, in electron-proton scattering. We have provided first estimates of the cross sections for exclusive production of χ_{cJ} quarkonia with positive C-parity at the EIC. This process requires a C-odd exchange in the t channel. In the limit of heavy quarks and/or high-transverse momentum transfer this could be the exchange of a photon, a Primakoff process, or the exchange of a color-symmetric three-gluon ladder, the odderon. Our estimates suggest that for $|t| \approx 1$ GeV^2 the two amplitudes are of similar magnitude and that there are strong interference effects. Importantly, the relative phase is not affected by QCD evolution of the odderon towards small x, and so it is determined by the three-gluon exchange amplitude at moderately small x_0. In turn, the matrix element of the eikonal color current operator $d^{abc} J^{+a} J^{+b} J^{+c}$ at x_0, for transverse momenta of order $\max(R_{\chi_c}^{-1}, |t|^{1/2})$ (R_{χ_c} being here roughly the size of χ_c), can be computed in a truncated Fock space for the proton that encompasses the states that are relevant in that kinematic regime.

We find that photon and odderon exchanges interfere constructively, leading to an enhancement of the differential

cross section for χ_{cJ} production around $|t| \approx 1$ GeV^2 by up to a factor of 4 over the pure photon exchange contribution. Given that both the normalization and the t dependence of the Primakoff process are reasonably well determined, this presents a very exciting opportunity to potentially discover at the EIC the hard C-odd exchange predicted by QCD. Furthermore, we find that towards top EIC energy, $\sqrt{S} = 140$ GeV, the total electroproduction cross section of χ_{cJ} quarkonia (with kinematic cuts specified in the previous section) levels off as neither photon nor odderon exchange involves a positive intercept. Therefore, it would be important to measure the energy dependence [89] of the cross section from $\sqrt{S} = 50$ GeV up to top EIC energy $\sqrt{S} = 140$ GeV, where photon and odderon amplitudes are similar, and where constructive interference of amplitudes leads to a total cross section for production of χ_{c1} and χ_{c2} quarkonia which exceeds the Primakoff component by a factor of ≈ 3–4.

The predictions for the odderon exchange process of course involve a number of uncertainties such as the matrix element in the proton of $d^{abc}J^{+a}J^{+b}J^{+c}$ or the value of the strong coupling α_S. The associated cross section scales approximately like α_S^6. Most importantly, the discovery of the hard QCD C-odd exchange requires fixing the normalization of the Primakoff background from measurements at low $\sqrt{|t|} < 0.5$ GeV; the relation (44) of the $t \to 0$ limit of the cross section to the $\gamma\gamma$ decay width provides an important constraint on theoretical predictions for this background. The t dependence of the Primakoff cross section is then determined by the Dirac and Pauli electromagnetic form factors of the proton which are well known. Hence, one may then look for excess events above this background, and for a change of slope of the differential cross section $d\sigma/dt$, at higher $|t| \sim 1$ GeV^2 and beyond.

Our estimates indicate very weak dipole-proton (hard) scattering with C-odd exchange; this is largely since these amplitudes are also parity odd and vanish for impact parameter $\boldsymbol{b}_\perp \to 0$, unlike parity even amplitudes, as well as due to the fact that they fall off more rapidly towards large $\boldsymbol{b}_\perp$. The total electro-production cross section of χ_{cJ} quarkonia at top EIC energy is estimated to have a magnitude of 10–20 fb (for $J = 1$) and 60 fb (for $J = 2$). Thus, it was not possible to observe these processes at the HERA accelerator. However, in view of the projected high luminosity of the EIC, data collection over a time span of several months to a year may be sufficient for the discovery of the hard odderon. A promising alternative would be to allow low-mass excitations of the proton, while requiring a large rapidity gap to the $C = +1$ quarkonia. Such rapidity gap, diffractive processes have greater cross sections than exclusive ones. Furthermore, they would extend the reach to higher $|t|$ where odderon exchange would more clearly dominate over photon exchange.

APPENDIX A: COMPUTATION OF THE LIGHT-CONE WAVE FUNCTIONS

In order to compute the light-cone wave functions, the key element is a vertex contraction between spinors, e.g., $\bar{u}_h(k)\Gamma v_{\bar{h}}(k')$ (Γ is some general Dirac vertex). For the spinors we use the LB basis, defined through

$$
\begin{aligned}
u_h(k) &= \frac{1}{2^{1/4}\sqrt{k^-}}(\sqrt{2}k^- + \gamma^0 m + \boldsymbol{\alpha}_\perp \cdot \boldsymbol{k}_\perp)\chi_h \\
&= \frac{1}{2^{1/4}\sqrt{k^-}}(\sqrt{2}k^- + \gamma^0 m + \boldsymbol{k}_\perp\gamma^0)\chi_h, \\
v_h(k) &= \frac{1}{2^{1/4}\sqrt{k^-}}(\sqrt{2}k^- - \gamma^0 m + \boldsymbol{\alpha}_\perp \cdot \boldsymbol{k}_\perp)\chi_{-h} \\
&= \frac{1}{2^{1/4}\sqrt{k^-}}(\sqrt{2}k^- - \gamma^0 m + \boldsymbol{k}_\perp\gamma^0)\chi_{-h}, \quad (A1)
\end{aligned}
$$

where $\alpha^i = \gamma^0\gamma^i$. In accordance with the conventions used in this work, we have switched plus and minus light-cone coordinates in the above expression as compared to the original LB convention [47]. Thus the spinors χ_h are eigenstates of $\gamma^+\gamma^-$, namely

$$
\frac{1}{2}\gamma^+\gamma^-\chi_h = \chi_h, \qquad \frac{1}{2}\gamma^-\gamma^+\chi_h = 0. \quad (A2)
$$

Explicitly, we have $\chi_+ = (-1, 0, 1, 0)/\sqrt{2}$, $\chi_- = (0, 1, 0, 1)/\sqrt{2}$. The spinors (A1) can now be written as

$$
\begin{aligned}
u_h(k) &= \frac{1}{2^{1/4}\sqrt{k^-}}(\not{k} + m)\gamma^0\chi_h, \\
v_h(k) &= \frac{1}{2^{1/4}\sqrt{k^-}}(\not{k} - m)\gamma^0\chi_{-h}. \quad (A3)
\end{aligned}
$$

By defining a projection matrix

$$\chi_{h\bar{h}} \equiv \gamma^0 \chi_{-\bar{h}} \tilde{\chi}_h \gamma^0, \tag{A4}$$

one obtains

$$\bar{u}_h(k)\Gamma v_{\bar{h}}(k') = \frac{1}{\sqrt{2k^- k'^-}} \text{tr}[(\not{k} + m)\Gamma(\not{k}' - m)\chi_{h\bar{h}}], \tag{A5}$$

and so the computation of the light-cone wave function comes down to the computation of the above Dirac trace. We use this method to compute all the wave functions considered in this work. Using (A4), the explicit forms of the projection matrices are found to be

$$\chi_{\pm\pm} = \pm \frac{1}{2\sqrt{2}} \gamma^-(\gamma^1 \mp i\gamma^2),$$

$$\chi_{\pm\mp} = \frac{1}{2\sqrt{2}} \gamma^-(1 \mp \gamma_5). \tag{A6}$$

APPENDIX B: DERIVATION OF THE AMPLITUDES FOR AXIAL AND TENSOR QUARKONIA

In this appendix we present the steps of the derivation of the amplitudes from Sec. II B for the axial-vector and tensor quarkonia.

In the case of axial quarkonia we plug the second line of (9) into the traces in (19) to obtain

$$A_{\lambda=0,\bar{\lambda}=0}(\boldsymbol{l}_\perp, \boldsymbol{l}_{1\perp}, z) = 0,$$

$$A_{\lambda=0,\bar{\lambda}=\pm}(\boldsymbol{l}_\perp, \boldsymbol{l}_{1\perp}, z) = 4Qz\bar{z}(\boldsymbol{\epsilon}_\perp^{\bar{\lambda}*} \times \boldsymbol{l}_{1\perp}),$$

$$A_{\lambda=\pm,\bar{\lambda}=0}(\boldsymbol{l}_\perp, \boldsymbol{l}_{1\perp}, z) = \frac{4}{M_{\mathcal{A}}}(m_c^2(\boldsymbol{\epsilon}_\perp^\lambda \times \boldsymbol{l}_{1\perp}) + l_{1\perp}^2(\boldsymbol{\epsilon}_\perp^\lambda \times \boldsymbol{l}_\perp)),$$

$$A_{\lambda=\pm,\bar{\lambda}=\pm}(\boldsymbol{l}_\perp, \boldsymbol{l}_{1\perp}, z) = 2(z - \bar{z})((\boldsymbol{\epsilon}_\perp^\lambda \cdot \boldsymbol{\epsilon}_\perp^{\bar{\lambda}*})(\boldsymbol{l}_\perp \times \boldsymbol{l}_{1\perp})$$
$$- (\boldsymbol{l}_\perp \cdot \boldsymbol{l}_{1\perp} + m_c^2)(\boldsymbol{\epsilon}_\perp^\lambda \times \boldsymbol{\epsilon}_\perp^{\bar{\lambda}*})). \tag{B1}$$

The last line is understood to contain four different combinations of photon and quarkonia transverse

polarizations. We used the following notations for the 2D cross products: $\boldsymbol{x}_\perp \times \boldsymbol{y}_\perp \equiv x^1 y^2 - x^2 y^1 = -\epsilon^{+-}\boldsymbol{x}_\perp \boldsymbol{y}_\perp$. The nonzero reduced amplitudes are

$$\mathcal{A}_{\lambda=0,\bar{\lambda}=\pm}(\boldsymbol{r}_\perp, \boldsymbol{\Delta}_\perp) = eq_c e^{-i\bar{\lambda}\phi_r} \int_z e^{-i\boldsymbol{\delta}_\perp \cdot \boldsymbol{r}_\perp} \mathcal{A}_{LT}(r_\perp),$$

$$\mathcal{A}_{\lambda=\pm,\bar{\lambda}=0}(\boldsymbol{r}_\perp, \boldsymbol{\Delta}_\perp) = eq_c e^{i\lambda\phi_r} \int_z e^{-i\boldsymbol{\delta}_\perp \cdot \boldsymbol{r}_\perp} \mathcal{A}_{TL}(r_\perp),$$

$$\mathcal{A}_{\lambda=\pm,\bar{\lambda}=\pm}(\boldsymbol{r}_\perp, \boldsymbol{\Delta}_\perp) = eq_c \lambda\delta_{\lambda\bar{\lambda}} \int_z e^{-i\boldsymbol{\delta}_\perp \cdot \boldsymbol{r}_\perp} \mathcal{A}_{TT}(r_\perp), \tag{B2}$$

where $\mathcal{A}_A$ are given in Eq. (29). Notice that the first term from the fourth line of (B1) is proportional to $\boldsymbol{r}_\perp \times \boldsymbol{r}_\perp = 0$ in coordinate space and so it does not contribute to $\mathcal{A}_{TT}(r_\perp)$. In the last line of Eq. (B2), out of four possible combinations of photon and axial quarkonia transverse polarizations, only the two polarization preserving transitions survive since this amplitude is proportional to the 2D cross product, $\boldsymbol{\epsilon}_\perp^\lambda \times \boldsymbol{\epsilon}_\perp^{\bar{\lambda}*} = (-i/2)(\lambda + \bar{\lambda}) = -i\lambda\delta_{\lambda\bar{\lambda}}$ of the polarization vectors of the incoming photon and outgoing axial-vector quarkonia. Accordingly, the two polarization flipping transitions vanish, unlike in case of vector quarkonia.

Computing now the ϕ_r integral we separate the helicity dependence and obtain the amplitudes

$$\langle \mathcal{M}_{\lambda=0,\bar{\lambda}=\pm 1} \rangle \equiv q^- \tilde{\mathcal{M}}_{0,\bar{\lambda}=\pm 1} \equiv q^- e^{-i\bar{\lambda}\phi_\Delta} \tilde{\mathcal{M}}_{LT},$$

$$\langle \mathcal{M}_{\lambda=\pm 1,\lambda=0} \rangle \equiv q^- \tilde{\mathcal{M}}_{\lambda=\pm 1,0} \equiv q^- e^{i\lambda\phi_\Delta} \tilde{\mathcal{M}}_{TL},$$

$$\langle \mathcal{M}_{\lambda=\pm 1,\bar{\lambda}=\pm 1} \rangle \equiv q^- \tilde{\mathcal{M}}_{\lambda=\pm 1,\bar{\lambda}=\pm 1} \equiv q^- \lambda\delta_{\lambda\bar{\lambda}} \tilde{\mathcal{M}}_{TT}, \tag{B3}$$

where $\tilde{\mathcal{M}}_B$ are given in Eq. (28).

For the tensor quarkonia, we proceed along similar steps as above, only this time there is a total of 15 overlaps that need to be computed. Starting from the traces (19), we plug in the third line of (9) and find

$$A_{\lambda=0,\bar{\lambda}=\pm 2}(\boldsymbol{l}_\perp, \boldsymbol{l}_{1\perp}, z) = -8Qz\bar{z}(z - \bar{z})(\boldsymbol{\epsilon}_\perp^{\pm*} \cdot \boldsymbol{l}_{1\perp})^2,$$

$$A_{\lambda=\pm 1,\bar{\lambda}=\pm 2}(\boldsymbol{l}_\perp, \boldsymbol{l}_{1\perp}, z) = -4(\boldsymbol{\epsilon}_\perp^{\pm*} \cdot \boldsymbol{l}_{1\perp})[(\boldsymbol{\epsilon}_\perp^\lambda \cdot \boldsymbol{\epsilon}_\perp^{\pm*})(\boldsymbol{l}_\perp \cdot \boldsymbol{l}_{1\perp} + m_c^2)$$
$$+ (z - \bar{z})^2(\boldsymbol{\epsilon}_\perp^\lambda \cdot \boldsymbol{l}_\perp)(\boldsymbol{\epsilon}_\perp^{\pm*} \cdot \boldsymbol{l}_{1\perp}) - (\boldsymbol{\epsilon}_\perp^\lambda \cdot \boldsymbol{l}_{1\perp})(\boldsymbol{\epsilon}_\perp^{\pm*} \cdot \boldsymbol{l}_\perp)],$$

$$A_{\lambda=0,\bar{\lambda}=\pm 1}(\boldsymbol{l}_\perp, \boldsymbol{l}_{1\perp}, z) = 2\sqrt{2}QM_{\mathcal{T}}z\bar{z}(3 - 4(z^2 + \bar{z}^2))(\boldsymbol{\epsilon}_\perp^{\bar{\lambda}} \cdot \boldsymbol{l}_{1\perp}),$$

$$A_{\lambda=\pm 1,\bar{\lambda}=\pm 1}(\boldsymbol{l}_\perp, \boldsymbol{l}_{1\perp}, z) = -\sqrt{2}M_{\mathcal{T}}(z - \bar{z})[(\boldsymbol{\epsilon}_\perp^\lambda \cdot \boldsymbol{\epsilon}_\perp^{\bar{\lambda}*})(\boldsymbol{l}_\perp \cdot \boldsymbol{l}_{1\perp} + m_c^2)$$
$$- (3 - 4(z^2 + \bar{z}^2))(\boldsymbol{\epsilon}_\perp^\lambda \cdot \boldsymbol{l}_\perp)(\boldsymbol{\epsilon}_\perp^{\bar{\lambda}*} \cdot \boldsymbol{l}_{1\perp}) - (\boldsymbol{\epsilon}_\perp^\lambda \cdot \boldsymbol{l}_{1\perp})(\boldsymbol{\epsilon}_\perp^{\bar{\lambda}*} \cdot \boldsymbol{l}_\perp)],$$

$$A_{\lambda=0,\bar{\lambda}=0}(\boldsymbol{l}_\perp, \boldsymbol{l}_{1\perp}, z) = \frac{8\sqrt{2}Q}{\sqrt{3}}z\bar{z}(z - \bar{z})\left(\frac{3}{2}l_{1\perp}^2 + m_c^2\right),$$

$$A_{\lambda=\pm 1,\bar{\lambda}=0}(\boldsymbol{l}_\perp, \boldsymbol{l}_{1\perp}, z) = \frac{2\sqrt{2}}{\sqrt{3}}\left[2(z - \bar{z})^2(\boldsymbol{\epsilon}_\perp^\lambda \cdot \boldsymbol{l}_\perp)\left(\frac{3}{2}l_{1\perp}^2 + m_c^2\right) + (\boldsymbol{\epsilon}_\perp^\lambda \cdot \boldsymbol{l}_{1\perp})m_c^2\right]. \tag{B4}$$

The results for $\bar{\lambda} = 0$ have been simplified using

$$(\boldsymbol{\epsilon}_\perp^{+*} \cdot \boldsymbol{u}_\perp)(\boldsymbol{\epsilon}_\perp^{-*} \cdot \boldsymbol{v}_\perp) + (\boldsymbol{\epsilon}_\perp^{-*} \cdot \boldsymbol{u}_\perp)(\boldsymbol{\epsilon}_\perp^{+*} \cdot \boldsymbol{v}_\perp) = -\boldsymbol{u}_\perp \cdot \boldsymbol{v}_\perp, \tag{B5}$$

which holds for general 2D vectors $\boldsymbol{u}_\perp$ and $\boldsymbol{v}_\perp$. Inserting (B4) in (18) we obtain the reduced amplitudes

$$\mathcal{A}_{\lambda=0,\bar{\lambda}=\pm2}(\boldsymbol{r}_\perp, \boldsymbol{\Delta}_\perp) = eq_c e^{-i\bar{\lambda}\phi_r} \int_z e^{-i\boldsymbol{\delta}_\perp \cdot \boldsymbol{r}_\perp} \mathcal{A}_{LT2}(r_\perp),$$

$$\mathcal{A}_{\lambda=\pm1,\bar{\lambda}=\pm2}(\boldsymbol{r}_\perp, \boldsymbol{\Delta}_\perp) = eq_c \lambda e^{i(\lambda-\bar{\lambda})\phi_r} \int_z e^{-i\boldsymbol{\delta}_\perp \cdot \boldsymbol{r}_\perp} (\delta_{\lambda,\bar{\lambda}/2}\mathcal{A}_{TT2p}(r_\perp) + \delta_{\lambda,-\bar{\lambda}/2}\mathcal{A}_{TT2f}(r_\perp)),$$

$$\mathcal{A}_{\lambda=0,\bar{\lambda}=\pm1}(\boldsymbol{r}_\perp, \boldsymbol{\Delta}_\perp) = eq_c \bar{\lambda} e^{-i\bar{\lambda}\phi_r} \int_z e^{-i\boldsymbol{\delta}_\perp \cdot \boldsymbol{r}_\perp} \mathcal{A}_{LT}(r_\perp),$$

$$\mathcal{A}_{\lambda=\pm1,\bar{\lambda}=\pm1}(\boldsymbol{r}_\perp, \boldsymbol{\Delta}_\perp) = eq_c e^{i(\lambda-\bar{\lambda})\phi_r} \int_z e^{-i\boldsymbol{\delta}_\perp \cdot \boldsymbol{r}_\perp} (\delta_{\lambda\bar{\lambda}}\mathcal{A}_{TTp}(r_\perp) - \delta_{\lambda,-\bar{\lambda}}\mathcal{A}_{TTf}(r_\perp)),$$

$$\mathcal{A}_{\lambda=0,\bar{\lambda}=0}(\boldsymbol{r}_\perp, \boldsymbol{\Delta}_\perp) = eq_c \int_z e^{-i\boldsymbol{\delta}_\perp \cdot \boldsymbol{r}_\perp} \mathcal{A}_{LL}(r_\perp),$$

$$\mathcal{A}_{\lambda=\pm1,\bar{\lambda}=0}(\boldsymbol{r}_\perp, \boldsymbol{\Delta}_\perp) = eq_c \lambda e^{i\lambda\phi_r} \int_z e^{-i\boldsymbol{\delta}_\perp \cdot \boldsymbol{r}_\perp} \mathcal{A}_{TL}(r_\perp). \tag{B6}$$

From (B6) we see that for the transverse polarizations of the photon and the tensor quarkonia both the polarization-preserving ($\lambda \to \bar{\lambda}/2$, for the case $\bar{\lambda} = \pm2$ and $\lambda \to \bar{\lambda}$ for the case $\bar{\lambda} = \pm1$) and polarization-flipped ($\lambda \to -\bar{\lambda}/2$, $\lambda \to -\bar{\lambda}$) transitions are allowed, which explains the notation (p = preserving, f = flipped).

In the final step we compute the amplitudes

$$\langle\mathcal{M}_{\lambda=0,\bar{\lambda}=\pm2}\rangle \equiv q^- \tilde{\mathcal{M}}_{\lambda=0,\bar{\lambda}=\pm2} \equiv q^- e^{-i\bar{\lambda}\phi_\Delta} \tilde{\mathcal{M}}_{LT2},$$

$$\langle\mathcal{M}_{\lambda=\pm1,\bar{\lambda}=\pm2}\rangle \equiv q^- \tilde{\mathcal{M}}_{\lambda=\pm1,\bar{\lambda}=\pm2} \equiv q^- \lambda e^{-i\lambda\phi_\Delta}\delta_{\lambda,\bar{\lambda}/2} \tilde{\mathcal{M}}_{TT2p} + q^- \lambda e^{3i\lambda\phi_\Delta}\delta_{\lambda,-\bar{\lambda}/2} \tilde{\mathcal{M}}_{TT2f},$$

$$\langle\mathcal{M}_{\lambda=0,\bar{\lambda}=\pm1}\rangle \equiv q^- \tilde{\mathcal{M}}_{\lambda=0,\bar{\lambda}=\pm1} \equiv q^- e^{-i\bar{\lambda}\phi_\Delta} \tilde{\mathcal{M}}_{LT},$$

$$\langle\mathcal{M}_{\lambda=\pm1,\bar{\lambda}=\pm1}\rangle \equiv q^- \tilde{\mathcal{M}}_{\lambda=\pm1,\bar{\lambda}=\pm1} \equiv q^- \delta_{\lambda\bar{\lambda}} \tilde{\mathcal{M}}_{TTp} + q^- \delta_{\lambda,-\bar{\lambda}} e^{2i\lambda\phi_\Delta} \tilde{\mathcal{M}}_{TTf},$$

$$\langle\mathcal{M}_{\lambda=0,\bar{\lambda}=0}\rangle \equiv q^- \tilde{\mathcal{M}}_{\lambda=0,\bar{\lambda}=0} \equiv q^- \tilde{\mathcal{M}}_{LL},$$

$$\langle\mathcal{M}_{\lambda=\pm1,\bar{\lambda}=0}\rangle \equiv q^- \tilde{\mathcal{M}}_{\lambda=\pm1,\bar{\lambda}=0} \equiv q^-(\delta_{\lambda1} - \delta_{\lambda,-1}) e^{i\lambda\phi_\Delta} \tilde{\mathcal{M}}_{TL}, \tag{B7}$$

where the explicit helicity dependence was also factored out. The scalar functions $\tilde{\mathcal{M}}_B$ are given by Eq. (31).

APPENDIX C: THE PRIMAKOFF CONTRIBUTION IN SPECIFIC KINEMATIC LIMITS

1. The proof of formula (44)

We begin by considering the amplitude for the decay process $\mathcal{H}(\bar{\lambda}, \Delta) \to \gamma(\lambda, q)\gamma(\lambda', \ell)$, where $\mathcal{H} = \mathcal{S}, \mathcal{T}$. In what follows, it will be useful to separate out the exchanged photon polarization from the amplitude as

$$\mathcal{M}_{\lambda\lambda'\bar{\lambda}}(\mathcal{H} \to \gamma\gamma) = \epsilon_\mu(\lambda', \ell)\mathcal{M}_{\lambda\bar{\lambda}}^\mu(\mathcal{H} \to \gamma\gamma). \tag{C1}$$

Inserting (C1) into the standard formula for the decay width [34] we get

$$\Gamma(\mathcal{H} \to \gamma\gamma) = \frac{1}{2J+1} \frac{1}{32\pi M_\mathcal{H}} \sum_{\bar{\lambda}=-J}^{J} \sum_{\lambda\lambda'} |\mathcal{M}_{\lambda\lambda'\bar{\lambda}}(\mathcal{H} \to \gamma\gamma)|^2,$$

$$= -\frac{1}{2J+1} \frac{1}{32\pi M_\mathcal{H}} \sum_{\bar{\lambda}=-J}^{J} \sum_{\lambda} g_{ii'}\mathcal{M}_{\lambda\bar{\lambda}}^i(\mathcal{H} \to \gamma\gamma)$$

$$\times \mathcal{M}_{\lambda\bar{\lambda}}^{i'*}(\mathcal{H} \to \gamma\gamma). \tag{C2}$$

Next, we consider the amplitude for exclusive photoproduction $\mathcal{M}_{\lambda\bar{\lambda}}(\gamma p \to \mathcal{H} p)$; see (50). The cross section reads [34]

$$\frac{d\sigma_\mathcal{H}(\gamma p \to \mathcal{H} p)}{d|t|}$$

$$= \frac{1}{2} \sum_{\bar{\lambda}=-J}^{J} \sum_{\lambda} \int \frac{d\phi_\ell}{2\pi} \frac{1}{16\pi W^4} |\mathcal{M}_{\lambda\bar{\lambda}}(\gamma p \to \mathcal{H} p)|^2, \tag{C3}$$

where $W^2 = (q+P)^2 \simeq 2q \cdot P \gg M_{\mathcal{H}}^2, P^2, |\ell^2|$ in the high-energy limit.[14] Moreover $\ell \approx (x_{\mathcal{P}} P^+, 0, \boldsymbol{\ell}_\perp)$ with ϕ_ℓ the azimuthal angle of $\boldsymbol{\ell}_\perp$. We also have $x_{\mathcal{P}} \approx M_{\mathcal{H}}^2/W^2$ [see Eq. (66)], and $\ell^2 = t \approx -\boldsymbol{\ell}_\perp^2$.

Taking the high-energy limit leads to (51). Here we pick up the leading F_1 term when $W^2 \gg |t|$

$$\mathcal{M}_{\lambda\bar{\lambda}}(\gamma p \to \mathcal{H}p)$$
$$= P_\mu \mathcal{M}_{\lambda\bar{\lambda}}^\mu(\gamma\gamma \to \mathcal{H}) \frac{eF_1(\ell_\perp)}{\ell^2} \frac{1}{q \cdot P} \bar{u}(P') \not{q} u(P). \quad (C4)$$

To make the connection (44) we rewrite (C4) using QED gauge invariance $\ell_\mu \mathcal{M}_{\lambda\bar{\lambda}}^\mu(\gamma\gamma \to \mathcal{H}) = 0$ in the high-energy limit (the Collins–Ellis trick [90])

$$P_\mu \mathcal{M}_{\lambda\bar{\lambda}}^\mu(\gamma\gamma \to \mathcal{H}) \approx -\frac{1}{x_{\mathcal{P}}} \ell_i \mathcal{M}_{\lambda\bar{\lambda}}^i(\gamma\gamma \to \mathcal{H}), \quad (C5)$$

so that

$$\mathcal{M}_{\lambda\bar{\lambda}}(\gamma p \to \mathcal{H}p) = -\frac{2eF_1(\ell_\perp)}{t} \frac{W^2}{M_{\mathcal{H}}^2} \ell_i \mathcal{M}_{\lambda\bar{\lambda}}^i(\gamma\gamma \to \mathcal{H}). \quad (C6)$$

Finally, the result in (C3) is isotropic in ϕ_ℓ after the polarization sum. We can perform the angular average leading to

$$\frac{1}{2} \sum_{\bar{\lambda}=-J}^{J} \sum_\lambda \int \frac{d\phi_\ell}{2\pi} |\ell_i \mathcal{M}_{\lambda\bar{\lambda}}^i(\gamma\gamma \to \mathcal{H})|^2$$
$$= -\frac{1}{4} \boldsymbol{\ell}_\perp^2 \sum_{\bar{\lambda}=-J}^{J} \sum_\lambda g_{ii'} \mathcal{M}_{\lambda\bar{\lambda}}^i(\gamma\gamma \to \mathcal{H}) \mathcal{M}_{\lambda\bar{\lambda}}^{i'*}(\gamma\gamma \to \mathcal{H})$$
$$= (2J+1) 8\pi M_{\mathcal{H}} \boldsymbol{\ell}_\perp^2 \Gamma(\mathcal{H} \to \gamma\gamma), \quad (C7)$$

where in the last line we used (C2). Inserting (C7) into (C3) via (C6) gives Eq. (44), which is the desired result. In the derivation we assumed scattering off a proton target, but the formula is valid for any charged particle.

2. The $|t| \to 0$ limit for axial-vector quarkonia and its connection to the Landau–Yang theorem

Thanks to the Collins–Ellis trick, the $\gamma^*\gamma^* \to \mathcal{H}$ amplitude for scalar and tensor quarkonia has a finite $O(\Delta_\perp)$ contribution. The Collins–Ellis trick is a rather general and robust procedure in the high-energy limit and so from this perspective the case of axial quarkonia seems special in that the $O(\Delta_\perp)$ contribution vanishes, with the amplitude scaling as $O(\Delta_\perp^2)$; check (47). In the following we demonstrate that $O(\Delta_\perp^2)$ scaling follows from a general

---

[14]The amplitudes $\mathcal{M}_{\lambda\bar{\lambda}}$ in this section and the amplitudes $\tilde{\mathcal{M}}_{\lambda\bar{\lambda}}$ of Eqs. (23), (B3), and (B7) are related through $\tilde{\mathcal{M}}_{\lambda\bar{\lambda}} = \mathcal{M}_{\lambda\bar{\lambda}}/W^2$; compare (C3) with (35).

argument which does not rely on a particular choice of axial-quarkonium wave function.

We take Eq. (41) as a starting point and further factor out the polarization vectors from the helicity amplitude as

$$n_\nu \mathcal{M}_{\lambda\bar{\lambda}}^\nu(\gamma^*\gamma^* \to \mathcal{A}) = \epsilon_\mu(\lambda, q) n_\nu E_\rho(\bar{\lambda}, \Delta_0) \mathcal{M}^{\mu\nu\rho}(\gamma^*\gamma^* \to \mathcal{A}). \quad (C8)$$

The covariant amplitude $\mathcal{M}^{\mu\nu\rho}(\gamma^*\gamma^* \to \mathcal{A})$ depends only on the vectors q^μ and ℓ^ν. Because $\mathcal{A}$ is an axial-vector quarkonium, $\mathcal{M}^{\mu\nu\rho}(\gamma^*\gamma^* \to \mathcal{A})$ has to be proportional to the ϵ tensor. In general the covariant decomposition is as follows:

$$\mathcal{M}^{\mu\nu\rho}(\gamma^*\gamma^* \to \mathcal{A}) = \left(q^\rho - \ell^\rho + \frac{-q^2 + \ell^2}{(q+\ell)^2}(q^\rho + \ell^\rho) \right)$$
$$\times \epsilon^{\mu\nu q\ell} M_{\mathcal{A}} F_{TT}(q^2, \ell^2)$$
$$+ \left(\ell^\mu - \frac{q \cdot \ell}{q^2} q^\mu \right) \epsilon^{\nu\rho q\ell} \sqrt{-q^2} F_{LT}(q^2, \ell^2)$$
$$+ \left(q^\nu - \frac{q \cdot \ell}{\ell^2} \ell^\nu \right) \epsilon^{\mu\rho q\ell} \sqrt{-\ell^2} F_{TL}(q^2, \ell^2) \quad (C9)$$

(see, e.g., [60] and references therein). The decomposition (C9) is QED gauge invariant, that is, $q_\mu \mathcal{M}^{\mu\nu\rho}(\gamma^*\gamma^* \to \mathcal{A}) = 0$ and $\ell_\nu \mathcal{M}^{\mu\nu\rho}(\gamma^*\gamma^* \to \mathcal{A}) = 0$, and we also have $(q^\rho + l^\rho) \mathcal{M}_{\mu\nu\rho}(\gamma^*\gamma^* \to \mathcal{A}) = 0$. Here the notation F_{TT}, F_{TL}, and F_{LT} refers to the $\gamma^*\gamma^*$ polarizations in the center-of-mass frame. Only the form-factor F_{TT} is constrained by the LY theorem $F_{TT}(0, 0) = 0$ [76,77]; see also Ref. [60]. Due to the Bose symmetry of the full amplitude (C9) we must have $F_{TT}(q^2, \ell^2) = -F_{TT}(\ell^2, q^2)$ and so $F_{TT}(q^2, \ell^2) \propto q^2 - \ell^2$ for small q^2 and ℓ^2. On the other hand, the form-factors F_{LT} and F_{TL} scale as $F_{LT}(q^2, \ell^2) \propto \sqrt{-q^2}$, $F_{TL}(q^2, \ell^2) \propto \sqrt{-\ell^2}$ in order to avoid kinematic singularities [60,91].

Contracting (C9) with the longitudinal polarization vector $E^\rho(0, \Delta_0)$, only the piece proportional to the gauge vector n^ρ from (12) survives. Further contracting with the transverse photon polarization $\epsilon^\mu(\lambda = \pm 1, q)$ and the gauge vector n^ν we obtain

$$n_\nu \mathcal{M}_{\lambda=\pm1,\bar{\lambda}=0}^\nu(\gamma^*\gamma^* \to \mathcal{A})$$
$$= -\frac{M_0}{\Delta_0 \cdot n}(q \cdot n) \epsilon^{\epsilon(\lambda,q)nq\ell} \left[\left(1 - \frac{q^2 - \ell^2}{\Delta_0^2} \right) M_{\mathcal{A}} F_{TT}(q^2, \ell^2) \right.$$
$$\left. + \sqrt{-\ell^2} F_{TL}(q^2, \ell^2) \right], \quad (C10)$$

where we have used $\ell \cdot n = 0$. The form-factor $F_{LT}(q^2, \ell^2)$ decouples after contracting $\epsilon^{\nu\rho ql}$ with $n_\nu E_\rho(0, \Delta_0)$. Taking into account the scalings of the form factors the square

bracket in (C10) is $O(\Delta_\perp^2)$ while the ϵ tensor is $O(\Delta_\perp)$ leading to the overall $O(\Delta_\perp^3)$ scaling.

For the transverse polarization we find

$$
\begin{aligned}
&n_\nu \mathcal{M}^\nu_{\lambda=\pm 1, \bar\lambda=\pm 1}(\gamma^* \gamma^* \to \mathcal{A}) \\
&= (q - l) \cdot E(\bar\lambda, \Delta_0) \epsilon^{\epsilon(\lambda, q) n q \ell} M_\mathcal{A} F_{TT}(q^2, \ell^2) \\
&\quad + (\epsilon(\lambda, q) \cdot \ell) \epsilon^{n E(\bar\lambda, \Delta_0) q \ell} \sqrt{-q^2} F_{LT}(q, \ell^2) \\
&\quad + (q \cdot n) \epsilon^{\epsilon(\lambda, q) E(\bar\lambda, \Delta_0) q \ell} \sqrt{-\ell^2} F_{TL}(q^2, \ell^2).
\end{aligned}
\tag{C11}
$$

The first term in (C11) is $O(\Delta_\perp^3)$, the second term decouples in the $q^2 \to 0$ limit, and the third term is $O(\Delta_\perp^2)$ which is the leading contribution in the $\Delta_\perp \to 0$ limit.

3. The NRQCD limit of the Primakoff cross sections

In this subsection we consider the nonrelativisitic QCD (NRQCD) limit of the Primakoff process by taking the heavy quark limit. We also take $Q^2 \to 0$ and focus on transverse photon-proton scattering.

In the NRQCD limit all the momenta in the amplitude are considered to be much smaller than the heavy quark mass. Since the expressions obtained in the Secs. C 1 and C 2 already correspond to the $|t| \to 0$ limit, we take those as a starting point and further expand to second order in $\xi = z - 1/2$ and $\boldsymbol{l}_\perp$.

For scalar quarkonia, using (46) we obtain

$$
\begin{aligned}
\tilde{\mathcal{M}}_T \to{}& 8\sqrt{2}\pi i q_c^2 \alpha N_c \frac{e F_1(\Delta_\perp)}{\Delta_\perp} \\
&\times \frac{1}{m_c^3} \int_z \int_{\boldsymbol{l}_\perp} (l_\perp^2 + 4\xi^2 m_c^2) \frac{\phi_\mathcal{S}(\boldsymbol{l}_\perp, z)}{z\bar z}.
\end{aligned}
\tag{C12}
$$

In the next step we replace the light-cone wave function (LCWF) $\phi_\mathcal{S}(\boldsymbol{l}_\perp, z)$ by the nonrelativistic radial wave function $u(l)$. Here $\boldsymbol{l} = (\boldsymbol{l}_\perp, l^3)$ and l is its modulus, with $l^3 = 2\xi m_c$ as appropriate for the NRQCD limit. The correspondence is given by [57]

$$
\int_z \int_{\boldsymbol{l}_\perp} \frac{\phi_\mathcal{S}(\boldsymbol{l}_\perp, z)}{z\bar z} \to \frac{1}{16\pi^2 \sqrt{m_c}} \frac{1}{\sqrt{N_c}} \int d^3 l \frac{u(l)}{l^2}.
\tag{C13}
$$

After performing the angular integrations in Eq. (C12) we relate $u(l)$ to the derivative of the radial wave function at the origin, as in Eq. (3.18) of Ref. [57]:

$$
\int_0^\infty dl\, l^2 u(l) = 3\sqrt{\frac{\pi}{2}} R'(0).
\tag{C14}
$$

This leads to

$$
\tilde{\mathcal{M}}_T \to 12\sqrt{\pi} i q_c^2 \alpha \sqrt{N_c} \frac{e F_1(\Delta_\perp)}{\Delta_\perp} \frac{1}{m_c^{7/2}} R'(0).
\tag{C15}
$$

The cross section is obtained from standard formulas; see Eq. (36). We find

$$
\frac{d\sigma(\gamma p \to \mathcal{S}p)}{d|t|} \to \frac{9\pi q_c^4 \alpha^3 N_c |R'(0)|^2 F_1^2(0)}{m_c^7 |t|}.
\tag{C16}
$$

The result agrees with Eq. (8b) of Jia *et al.* [88].

For axial-vector quarkonia there is an additional factor of $\sqrt{3/2}$ on the rhs of Eq. (C13). Recalling that the leading contribution in the $|t| \to 0$ limit comes from the amplitude $\tilde{\mathcal{M}}_{TT}$ of (47), and using (37), we find that in the NRQCD limit

$$
\frac{d\sigma(\gamma p \to \mathcal{A}p)}{d|t|} \to \frac{3\pi q_c^4 \alpha^3 N_c |R'(0)|^2 F_1^2(0)}{m_c^9},
\tag{C17}
$$

which also agrees with Eq. (8c) in Ref. [88].

For the tensor quarkonia with $\bar\lambda = \pm 1, \pm 2$, the rhs of Eq. (C13) is multiplied by a factor of $\sqrt{3}/M_\mathcal{T}$. Using (49) and (38) we find that the leading contribution comes from the amplitude $\tilde{\mathcal{M}}_{TT2,p}$ so that

$$
\frac{d\sigma(\gamma p \to \mathcal{T}p)}{d|t|} \to \frac{12\pi q_c^4 \alpha^3 N_c |R'(0)|^2 F_1^2(0)}{m_c^7 |t|}.
\tag{C18}
$$

This also agrees with Eq. (8d) in Ref. [88].

APPENDIX D: THE RELATIVE SIGN OF THE EIKONAL PHOTON AND ODDERON EXCHANGE AMPLITUDES

In this appendix we explain in detail our conventions for covariant derivatives, field equations, and Wilson lines. Consistent conventions are important for obtaining the correct relative sign of the Primakoff and odderon amplitudes.

We write the covariant derivative in the fundamental representation as

$$
(D^\mu)_{ij} = \delta_{ij}(\partial^\mu + i e q_c A^\mu) + i g A^{\mu a}(t^a)_{ij}.
\tag{D1}
$$

Here, $i, j = 1, \ldots, N_c$ are fundamental and $a = 1, \ldots, (N_c^2 - 1)$ is an adjoint color index; A^μ, $A^{\mu a}$ represent the electromagnetic and color fields, respectively, and t^a are the traceless generators of color-SU(N_c), normalized as $\mathrm{tr}(t^a t^b) = \frac{1}{2}\delta^{ab}$. q_c denotes the fractional electromagnetic charge of the fermion field on which this covariant derivative acts, $q_c = +2/3$ for c quarks.

From the Dirac equation for a massless fermion field, $i\gamma_\mu (D^\mu)_{ij} \psi_j = 0$, in a background with eikonal ("shock-wave") A^μ and $A^{\mu a}$ fields (where A^+ is the only nonvanishing field component and independent of x^+), ψ_j is proportional to the Wilson line

$$
\begin{aligned}
V(\boldsymbol{x}_\perp) = \mathcal{P} \exp\bigg\{ &-i \int_{-\infty}^{+\infty} dx^- [e q_c A^+(x^-, \boldsymbol{x}_\perp) \\
&+ g A^{+a}(x^-, \boldsymbol{x}_\perp) t^a] \bigg\}.
\end{aligned}
\tag{D2}
$$

The Yang–Mills and Maxwell equations for the shockwave fields in covariant gauge are

$$\partial_\mu F_a^{\mu\nu} = J_a^\nu \rightarrow -\mathbf{\nabla}_\perp^2 A_a^+ = J_a^+, \quad (D3)$$

$$\partial_\mu F^{\mu\nu} = J^\nu \rightarrow -\mathbf{\nabla}_\perp^2 A^+ = J^+, \quad (D4)$$

where J^{+a} and J^+ are the plus components of the color and electromagnetic currents, respectively. Note that here A^+ denotes the electromagnetic field sourced by the charges in the proton, from which the projectile $c\bar{c}$ dipole scatters.

We now define the S matrix for eikonal scattering of the color singlet dipole, averaged over the colors of the $c, \bar{c}$ quarks

$$S(\mathbf{x}_\perp, \mathbf{y}_\perp) = \frac{1}{N_c} \mathrm{tr}\langle V(\mathbf{x}_\perp) V^\dagger(\mathbf{y}_\perp)\rangle. \quad (D5)$$

$\langle \cdots \rangle$ denotes the matrix element of the respective operator between proton states $|P^+, \mathbf{P}_\perp\rangle$ and $\langle P^+ + \Delta^+, \mathbf{P}_\perp + \mathbf{\Delta}_\perp|$, stripped of the δ functions representing conservation of light-cone and transverse momentum.

We can now define the amplitudes for single photon or three-gluon exchange as follows. Setting the QCD coupling $g = 0$ and expanding the Wilson lines to linear order in A^+ we have

$$V(\mathbf{x}_\perp) = 1 - \mathrm{i}eq_c \int_{-\infty}^{+\infty} \mathrm{d}x^- A^+(x^-, \mathbf{x}_\perp)$$
$$\equiv 1 - \mathrm{i}eq_c\alpha(\mathbf{x}_\perp). \quad (D6)$$

Then,

$$\Omega(\mathbf{x}_\perp, \mathbf{y}_\perp) \equiv -\frac{1}{2\mathrm{i}}\langle V(\mathbf{x}_\perp)V^\dagger(\mathbf{y}_\perp) - V(\mathbf{y}_\perp)V^\dagger(\mathbf{x}_\perp)\rangle$$
$$= eq_c\langle\alpha(\mathbf{x}_\perp) - \alpha(\mathbf{y}_\perp)\rangle \quad (D7)$$

corresponds to the scattering amplitude for single photon exchange. With the field equation (D4) we can write $\langle\alpha(\mathbf{x}_\perp)\rangle = -\langle\frac{1}{\mathbf{\nabla}_\perp^2}\rho(\mathbf{x}_\perp)\rangle$ where the integrated electric charge density is $\rho(\mathbf{x}_\perp) = \int_{-\infty}^{+\infty} \mathrm{d}x^- J^+(x^-, \mathbf{x}_\perp)$. Performing a Fourier transform from the transverse coordinate to the transverse momentum space, the matrix element of this operator is simply the Dirac electromagnetic form factor of the proton, $eF_1(q_\perp^2) = \langle\rho(\mathbf{q}_\perp)\rangle$. This leads to

$$\Omega(\mathbf{r}_\perp, \mathbf{\Delta}_\perp) = 8\pi\mathrm{i}\alpha q_c \frac{F_1(\Delta_\perp^2)}{\Delta_\perp^2}\sin\left(\frac{\mathbf{r}_\perp \cdot \mathbf{\Delta}_\perp}{2}\right). \quad (D8)$$

Here we introduced $\mathbf{r}_\perp = \mathbf{x}_\perp - \mathbf{y}_\perp$. This is the expression written in Eq. (40) of the main text. In impact parameter space,

$$\Omega(\mathbf{r}_\perp, \mathbf{b}_\perp) = 8\pi\alpha q_c \int_{\mathbf{\Delta}_\perp} \sin(\mathbf{b}_\perp \cdot \mathbf{\Delta}_\perp)\frac{-F_1(\Delta_\perp^2)}{\Delta_\perp^2}\sin\left(\frac{\mathbf{r}_\perp \cdot \mathbf{\Delta}_\perp}{2}\right).$$
$$(D9)$$

We now proceed to the three-gluon exchange amplitude by setting $q_c = 0$ in the Wilson line (D2) followed by an expansion of (5), namely

$$\mathcal{O}(\mathbf{x}_\perp, \mathbf{y}_\perp) = -\frac{1}{2\mathrm{i}N_c}\mathrm{tr}\langle V(\mathbf{x}_\perp)V^\dagger(\mathbf{y}_\perp) - V(\mathbf{y}_\perp)V^\dagger(\mathbf{x}_\perp)\rangle,$$
$$(D10)$$

to third order in A^{+a}:

$$\mathcal{O}(\mathbf{r}_\perp, \mathbf{b}_\perp) = \frac{g^3}{4N_c}d^{abc}\int_{\mathbf{q}_{1\perp}\mathbf{q}_{2\perp}\mathbf{q}_{3\perp}} \frac{\langle\rho^a(\mathbf{q}_{1\perp})\rho^b(\mathbf{q}_{2\perp})\rho^c(\mathbf{q}_{3\perp})\rangle}{q_{1\perp}^2 q_{2\perp}^2 q_{3\perp}^2}$$
$$\times \sin(\mathbf{b}_\perp \cdot (\mathbf{q}_{1\perp} + \mathbf{q}_{2\perp} + \mathbf{q}_{3\perp}))$$
$$\times \left[\sin\left(\frac{1}{2}\mathbf{r}_\perp \cdot (\mathbf{q}_{1\perp} - \mathbf{q}_{2\perp} - \mathbf{q}_{3\perp})\right)\right.$$
$$\left. + \frac{1}{3}\sin\left(\frac{1}{2}\mathbf{r}_\perp \cdot (\mathbf{q}_{1\perp} + \mathbf{q}_{2\perp} + \mathbf{q}_{3\perp})\right)\right]. \quad (D11)$$

For details, see Eq. (77) of Ref. [23], to be multiplied by a factor of i [compare our Eq. (D10) to their Eq. (76)], and their Appendix B. Here $\rho^a(\mathbf{x}_\perp) = \int_{-\infty}^{+\infty} \mathrm{d}x^- J^{+a}(x^-, \mathbf{x}_\perp)$ denotes the color charge density integrated along the eikonal path. We now write the C-conjugation odd part of the color charge correlator as

$$\langle\rho^a(\mathbf{q}_{1\perp})\rho^b(\mathbf{q}_{2\perp})\rho^c(\mathbf{q}_{3\perp})\rangle = \frac{1}{4}d^{abc}g^3G_3^-(\mathbf{q}_{1\perp}, \mathbf{q}_{2\perp}, \mathbf{q}_{3\perp}).$$
$$(D12)$$

In a three-quark model this correlator takes the form [23]

$$G_3^-(\mathbf{q}_{1\perp}, \mathbf{q}_{2\perp}, \mathbf{q}_{3\perp}) = \int [\mathrm{d}x_i]\int [\mathrm{d}^2 p_i]\psi(x_1, \mathbf{p}_{1\perp}; x_2, \mathbf{p}_{2\perp}; x_3, \mathbf{p}_{3\perp})[\psi^*(x_1, \mathbf{p}_{1\perp} + (x_1 - 1)\mathbf{q}_\perp; x_2, \mathbf{p}_{2\perp} + x_2\mathbf{q}_\perp; x_3, \mathbf{p}_{3\perp} + x_3\mathbf{q}_\perp)$$
$$- \psi^*(x_1, \mathbf{p}_{1\perp} - \mathbf{q}_{1\perp} + x_1\mathbf{q}_\perp; x_2, \mathbf{p}_{2\perp} - \mathbf{q}_{2\perp} - \mathbf{q}_{3\perp} + x_2\mathbf{q}_\perp; x_3, \mathbf{p}_{3\perp} + x_3\mathbf{q}_\perp)$$
$$- \psi^*(x_1, \mathbf{p}_{1\perp} - \mathbf{q}_{1\perp} - \mathbf{q}_{3\perp} + x_1\mathbf{q}_\perp; x_2, \mathbf{p}_{2\perp} - \mathbf{q}_{2\perp} + x_2\mathbf{q}_\perp; x_3, \mathbf{p}_{3\perp} + x_3\mathbf{q}_\perp)$$
$$- \psi^*(x_1, \mathbf{p}_{1\perp} - \mathbf{q}_{1\perp} - \mathbf{q}_{2\perp} + x_1\mathbf{q}_\perp; x_2, \mathbf{p}_{2\perp} - \mathbf{q}_{3\perp} + x_2\mathbf{q}_\perp; x_3, \mathbf{p}_{3\perp} + x_3\mathbf{q}_\perp)$$
$$+ 2\psi^*(x_1, \mathbf{p}_{1\perp} - \mathbf{q}_{1\perp} + x_1\mathbf{q}_\perp; x_2, \mathbf{p}_{2\perp} - \mathbf{q}_{2\perp} + x_2\mathbf{q}_\perp; x_3, \mathbf{p}_{3\perp} - \mathbf{q}_{3\perp} + x_3\mathbf{q}_\perp)]. \quad (D13)$$

Here, $\boldsymbol{q}_\perp = \boldsymbol{q}_{1\perp} + \boldsymbol{q}_{2\perp} + \boldsymbol{q}_{3\perp}$ and

$$[dx_i] \equiv dx_1 dx_2 dx_3 \delta(1 - x_1 - x_2 - x_3),$$

$$[d^2 p_i] \equiv \frac{1}{(16\pi^3)^2} d^2\boldsymbol{p}_{1\perp} d^2\boldsymbol{p}_{2\perp} d^2\boldsymbol{p}_{3\perp} \delta^{(2)}(\boldsymbol{p}_{1\perp} + \boldsymbol{p}_{2\perp} + \boldsymbol{p}_{3\perp})$$

$$\text{(D14)}$$

denote integrations over the quark light-cone momentum fractions and transverse momenta. $\psi(x_1, \boldsymbol{p}_{1\perp}; x_2, \boldsymbol{p}_{2\perp}; x_3, \boldsymbol{p}_{3\perp})$ is the light-cone wave function of the model proton. This expression agrees with the C-odd three-gluon exchange proton impact factor $E_{3;0}$ by Bartels and Motyka [92] up to a conventional factor of $(-i)^3$. The first term in Eq. (D13) corresponds to the coupling of the three exchanged gluons to the same quark in the proton, and it is equal to the Dirac form factor $F_1(\boldsymbol{q}_\perp^2)$; note the opposite sign as compared to the photon exchange amplitude (D9). This contribution is dominant when all $|\boldsymbol{q}_{\perp i}|$ are much greater than the typical quark-transverse momentum while $|\boldsymbol{q}_\perp|$ is on the order of that scale. For high-momentum transfer $|t| = \boldsymbol{q}_\perp^2$ on the other hand, contributions due to gluon exchanges with two or three quarks in the proton become dominant. Where this transition occurs is determined by the light-cone wave function ψ which encodes the structure of the proton,

FIG. 8. The odderon amplitude $\mathcal{O}(\boldsymbol{r}_\perp, \boldsymbol{b}_\perp)$ obtained from a light-front quark model [66,67], when the relative angle between $\boldsymbol{r}_\perp$ and $\boldsymbol{b}_\perp$ $\phi_{rb} = 0$. At small $b_\perp$ the sign is negative.

specifically the single quark momentum distribution as well as multiquark momentum correlations.

G_3^- can also be expressed [93] in terms of two-gluon exchanges, $G_2(\boldsymbol{q}_{1\perp}, \boldsymbol{q}_{2\perp}) = 2\delta^{ab} \langle \rho^a(\boldsymbol{q}_{1\perp})\rho^b(\boldsymbol{q}_{2\perp})\rangle / g^2(N_c^2 - 1)$, where two of the three gluons are "paired up," plus a genuine three-body contribution which enforces the Ward identity (vanishing of G_3^-) when either one of the transverse momenta vanishes, $\boldsymbol{q}_{\perp i} \to 0$:

$$G_3^-(\boldsymbol{q}_{1\perp}, \boldsymbol{q}_{2\perp}, \boldsymbol{q}_{3\perp}) = G_2(\boldsymbol{q}_{1\perp} + \boldsymbol{q}_{2\perp}, \boldsymbol{q}_{3\perp}) + G_2(\boldsymbol{q}_{1\perp} + \boldsymbol{q}_{3\perp}, \boldsymbol{q}_{2\perp}) + G_2(\boldsymbol{q}_{2\perp} + \boldsymbol{q}_{3\perp}, \boldsymbol{q}_{1\perp})$$
$$- 2 \int [dx_i] \int [d^2 p_i][\psi^*(x_1, \boldsymbol{p}_{1\perp} + (x_1 - 1)\boldsymbol{q}_\perp; x_2, \boldsymbol{p}_{2\perp} + x_2\boldsymbol{q}_\perp; x_3, \boldsymbol{p}_{3\perp} + x_3\boldsymbol{q}_\perp)$$
$$- \psi^*(x_1, \boldsymbol{p}_{1\perp} - \boldsymbol{q}_{1\perp} + x_1\boldsymbol{q}_\perp; x_2, \boldsymbol{p}_{2\perp} - \boldsymbol{q}_{2\perp} + x_2\boldsymbol{q}_\perp; x_3, \boldsymbol{p}_{3\perp} - \boldsymbol{q}_{3\perp} + x_3\boldsymbol{q}_\perp)]$$
$$\times \psi(x_1, \boldsymbol{p}_{1\perp}; x_2, \boldsymbol{p}_{2\perp}; x_3, \boldsymbol{p}_{3\perp}). \quad \text{(D15)}$$

Once again, for small $|\boldsymbol{q}_\perp|$ but large $|\boldsymbol{q}_{\perp i}|$ the fourth term on the right-hand side of this equation becomes $-2F_1(\boldsymbol{q}_\perp^2)$.

A simple light-front quark model wave function from the literature [66,67] predicts $\mathcal{O}(\boldsymbol{r}_\perp, \boldsymbol{b}_\perp) < 0$ at small impact parameters; see Fig. 8. This corresponds to constructive interference of photon and odderon exchange amplitudes. Neither the fixed order $\mathcal{O}(\alpha_S)$ correction [65] to the matrix element $\langle \rho^a(\boldsymbol{q}_{1\perp})\rho^b(\boldsymbol{q}_{2\perp})\rho^c(\boldsymbol{q}_{3\perp})\rangle$ nor small-x resummation of $\mathcal{O}(\boldsymbol{r}_\perp, \boldsymbol{b}_\perp)$ change this initial sign; the resulting first harmonic $\mathcal{O}_1(\boldsymbol{r}_\perp, \Delta_\perp)$ at smaller x is shown above in Fig. 2.

Finally, let us mention that a third C-conjugation odd amplitude corresponds to the exchange of a single photon plus two gluons in a color singlet state. This corresponds to the expansion of Eq. (D5) to linear order in the electromagnetic and to quadratic order in the color field. This contribution is expected to be small [33] and has not been considered here.
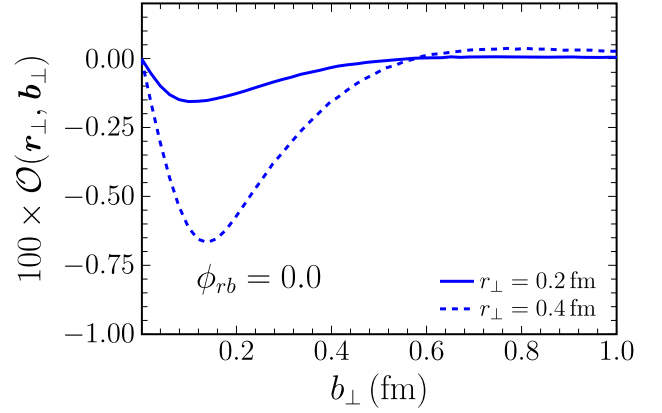
APPENDIX E: BJKP–BLV ODDERON

In this work the small-x evolution of the odderon exchange amplitude has been computed using the nonlinear evolution of the odderon coupled to the BK equation [11,12]—the "unitarized solution." It is interesting to compare to the BLV solution [9] obtained from the BKP equation for the odderon, that is, without including the unitarity corrections[15]—the "linear solution." Starting from the initial condition at $Y = 0$ obtained in [65] and described in Sec. II D, in Fig. 9 we show $\mathcal{O}_1(r_\perp, \Delta_\perp)$ as a function of $Y = \log(x_0/x_\mathcal{P})$ (left) with fixed $r_\perp = 0.3$ fm and $\Delta_\perp = 1$ GeV and up to $Y = 10$. The unitarized (full) and the linear (dashed line) results for $\mathcal{O}_1(r_\perp, \Delta_\perp)$ both drop as a function of Y. For the unitarized solution this is more

---

[15]Alternatively, one could solve for the BKP Green's function and reconstruct the odderon amplitude from it [94].
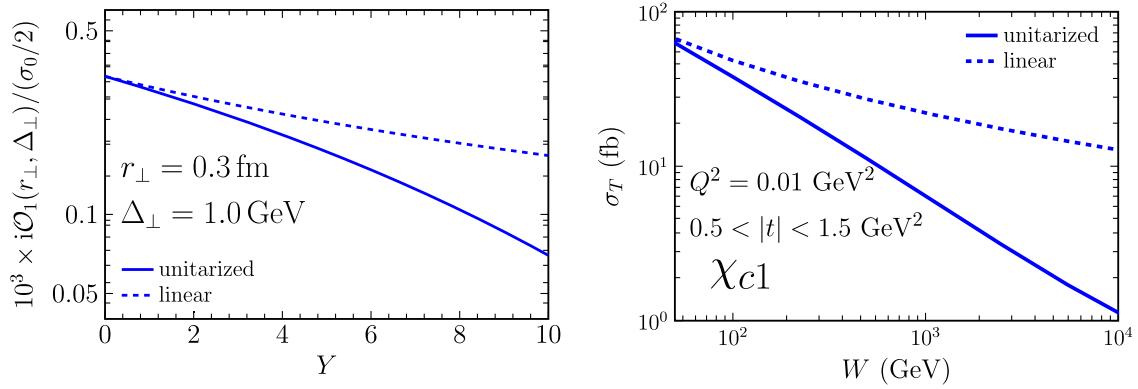
FIG. 9. Left: a comparison of the unitarized vs linear evolution of the odderon amplitude $\mathcal{O}_1(r_\perp, \Delta_\perp)$ as a function of Y. Right: a plot of the resulting W dependence of the odderon component of the $\gamma^* p \to \chi_{c1} p$ cross section.

pronounced due to the nonlinear corrections suppressing the odderon exchange amplitude [14,59,95].

The impact of the unitarized vs linear evolution on the W dependence of the odderon component of the cross section is shown in Fig. 9 (right). As an example, we consider the $\sigma_T(\gamma^* p \to \chi_{c1} p)$ cross section with the kinematic cuts as in Fig. 4 from which we reproduced the result of unitarized evolution. The range in Y shown in Fig. 9 (left) roughly translates to the range in W shown on the right. Even though linear evolution does lead to a much milder W dependence of σ_T, the cross section does not seem to fully reach the BLV asymptotics (a constant value) even for $W = 10^4$ GeV. Note, however, that from the standard saddle point analysis one expects a $1/Y^3$ correction to the asymptotic behavior of the

nonforward BLV exchange cross section, as established for the analogous case of the nonforward BFKL cross section [96]. From the perspective of the EIC, taking the top $\sqrt{S} = 140$ GeV collision energy of the ep system, W can reach at most $W \approx 136$ GeV (at $y = 0.95$) resulting in a factor of 2–3 difference in the cross section at the high y end of the photon flux. Due to the $1/y$ leading behavior of the photon flux, however, the exclusive χ_{cJ} production at the EIC will be dominated by much lower W, close to the experimental lower cutoff on W for exclusive events, say for $2 < Y < 4$, where the unitarity corrections to the odderon exchange cross section are below 30%, i.e., small in comparison to the theoretical uncertainty.

[1] L. Lukaszuk and B. Nicolescu, A possible interpretation of pp rising total cross-sections, Lett. Nuovo Cimento **8**, 405 (1973).

[2] J. Bartels, High-energy behavior in a non-Abelian gauge theory (II): First corrections to $T_{n \to m}$ beyond the leading ln s approximation, Nucl. Phys. **B175**, 365 (1980).

[3] J. Kwiecinski and M. Praszalowicz, Three gluon integral equation and odd c singlet Regge singularities in QCD, Phys. Lett. **94B**, 413 (1980).

[4] T. Jaroszewicz, Infrared divergences and Regge behavior in QCD, Acta Phys. Pol. B **11**, 965 (1980).

[5] L. N. Lipatov, Reggeization of the vector meson and the vacuum singularity in non-Abelian gauge theories, Sov. J. Nucl. Phys. **23**, 338 (1976).

[6] E. A. Kuraev, L. N. Lipatov, and V. S. Fadin, The Pomeranchuk singularity in non-Abelian gauge theories, Sov. Phys. JETP **45**, 199 (1977).

[7] I. I. Balitsky and L. N. Lipatov, The Pomeranchuk singularity in quantum chromodynamics, Sov. J. Nucl. Phys. **28**, 822 (1978).

[8] J. Bartels, V. S. Fadin, L. N. Lipatov, and G. P. Vacca, NLO corrections to the kernel of the BKP-equations, Nucl. Phys. **B867**, 827 (2013).

[9] J. Bartels, L. N. Lipatov, and G. P. Vacca, A new odderon solution in perturbative QCD, Phys. Lett. B **477**, 178 (2000).

[10] A. M. Stasto, Small x resummation and the Odderon, Phys. Lett. B **679**, 288 (2009).

[11] Y. V. Kovchegov, L. Szymanowski, and S. Wallon, Perturbative odderon in the dipole model, Phys. Lett. B **586**, 267 (2004).

[12] Y. Hatta, E. Iancu, K. Itakura, and L. McLerran, Odderon in the color glass condensate, Nucl. Phys. **A760**, 172 (2005).

[13] L. Motyka, Nonlinear evolution of pomeron and odderon in momentum space, Phys. Lett. B **637**, 185 (2006).

[14] T. Lappi, A. Ramnath, K. Rummukainen, and H. Weigert, JIMWLK evolution of the odderon, Phys. Rev. D **94**, 054014 (2016).

[15] X. Yao, Y. Hagiwara, and Y. Hatta, Computing the gluon Sivers function at small-x, Phys. Lett. B **790**, 361 (2019).

[16] C. Contreras, E. Levin, R. Meneses, and M. Sanhueza, QCD odderon: Nonlinear evolution in the leading twist, Phys. Rev. D **101**, 096019 (2020).

[17] S. Benić, D. Horvatić, A. Kaushik, and E. A. Vivoda, Exclusive η_c production from small-x evolved Odderon at an electron-ion collider, Phys. Rev. D **108**, 074005 (2023).

[18] S. Jeon and R. Venugopalan, A classical odderon in QCD at high energies, Phys. Rev. D **71**, 125003 (2005).

[19] S. Jeon and R. Venugopalan, Random walks of partons in SU(N(c)) and classical representations of color charges in QCD at small x, Phys. Rev. D **70**, 105012 (2004).

[20] J. Zhou, Transverse single spin asymmetries at small x and the anomalous magnetic moment, Phys. Rev. D **89**, 074050 (2014).

[21] R. Boussarie, Y. Hatta, L. Szymanowski, and S. Wallon, Probing the gluon sivers function with an unpolarized target: GTMD distributions and the odderons, Phys. Rev. Lett. **124**, 172501 (2020).

[22] Y. Hagiwara, Y. Hatta, R. Pasechnik, and J. Zhou, Spin-dependent Pomeron and Odderon in elastic proton-proton scattering, Eur. Phys. J. C **80**, 427 (2020).

[23] A. Dumitru, G. A. Miller, and R. Venugopalan, Extracting many-body color charge correlators in the proton from exclusive DIS at large Bjorken x, Phys. Rev. D **98**, 094004 (2018).

[24] A. Dumitru, H. Mäntysaari, and R. Paatelainen, Cubic color charge correlator in a proton made of three quarks and a gluon, Phys. Rev. D **105**, 036007 (2022).

[25] G. Antchev et al. (TOTEM Collaboration), Elastic differential cross-section $d\sigma/dt$ at $\sqrt{s} = 2.76$ TeV and implications on the existence of a colourless C-odd three-gluon compound state, Eur. Phys. J. C **80**, 91 (2020).

[26] V. M. Abazov et al. (D0 Collaboration), Measurement of the differential cross section $d\sigma/dt$ in elastic $p\bar{p}$ scattering at $\sqrt{s} = 1.96$ TeV, Phys. Rev. D **86**, 012009 (2012).

[27] A. Schafer, L. Mankiewicz, and O. Nachtmann, Diffractive $\eta_c, \eta', J/\psi$ and ψ' production in electron—proton collisions at HERA energies, in *Workshop on Physics at HERA* (Hamburg Deutsches Elektronen-Synchrotron, 1992).

[28] J. Czyzewski, J. Kwiecinski, L. Motyka, and M. Sadzikowski, Exclusive η_c photoproduction and electroproduction at HERA as a possible probe of the odderon singularity in QCD, Phys. Lett. B **398**, 400 (1997); **411**, 402 (E) (1997).

[29] R. Engel, D. Y. Ivanov, R. Kirschner, and L. Szymanowski, Diffractive meson production from virtual photons with odd charge—parity exchange, Eur. Phys. J. C **4**, 93 (1998).

[30] W. Kilian and O. Nachtmann, Single pseudoscalar meson production in diffractive ep scattering, Eur. Phys. J. C **5**, 317 (1998).

[31] E. R. Berger, A. Donnachie, H. G. Dosch, W. Kilian, O. Nachtmann, and M. Rueter, Odderon and photon exchange in electroproduction of pseudoscalar mesons, Eur. Phys. J. C **9**, 491 (1999).

[32] J. Bartels, M. A. Braun, D. Colferai, and G. P. Vacca, Diffractive η_c photoproduction and electroproduction with the perturbative QCD odderon, Eur. Phys. J. C **20**, 323 (2001).

[33] A. Dumitru and T. Stebel, Multiquark matrix elements in the proton and three gluon exchange for exclusive η_c production

[34] in photon-proton diffractive scattering, Phys. Rev. D **99**, 094038 (2019).

[34] R. L. Workman et al. (Particle Data Group), Review of particle physics, Prog. Theor. Exp. Phys. **2022**, 083C01 (2022).

[35] S. R. Klein, Comment on "η_c production in photon-induced interactions at the LHC", Phys. Rev. D **98**, 118501 (2018).

[36] L. A. Harland-Lang, V. A. Khoze, A. D. Martin, and M. G. Ryskin, Searching for the odderon in ultraperipheral proton–ion collisions at the LHC, Phys. Rev. D **99**, 034011 (2019).

[37] S. J. Brodsky, J. Rathsman, and C. Merino, Odderon-Pomeron interference, Phys. Lett. B **461**, 114 (1999).

[38] P. Hägler, B. Pire, L. Szymanowski, and O. V. Teryaev, Hunting the QCD-Odderon in hard diffractive electroproduction of two pions, Phys. Lett. B **535**, 117 (2002); **540**, 324(E) (2002).

[39] P. Hagler, B. Pire, L. Szymanowski, and O. V. Teryaev, Pomeron—odderon interference effects in electroproduction of two pions, Eur. Phys. J. C **26**, 261 (2002).

[40] A. Schafer, L. Mankiewicz, and O. Nachtmann, Double diffractive J/ψ and ϕ production as a probe for the odderon, Phys. Lett. B **272**, 419 (1991).

[41] A. Bzdak, L. Motyka, L. Szymanowski, and J. R. Cudell, Exclusive J/ψ and γ hadroproduction and the QCD odderon, Phys. Rev. D **75**, 094023 (2007).

[42] L. Pentchev et al. (GlueX Collaboration), Exclusive threshold J/ψ photoproduction with GlueX, in *Presented at DIS2023: XXX International Workshop on Deep-Inelastic Scattering and Related Subjects* (Michigan State University, East Lansing, Michigan, USA, 2023).

[43] A. Accardi et al., Electron Ion Collider: The next QCD frontier: Understanding the glue that binds us all, Eur. Phys. J. A **52**, 268 (2016).

[44] R. Abdul Khalek et al., Science requirements and detector concepts for the electron-ion collider: EIC Yellow Report, Nucl. Phys. **A1026**, 122447 (2022).

[45] N. N. Nikolaev and B. G. Zakharov, Color transparency and scaling properties of nuclear shadowing in deep inelastic scattering, Z. Phys. C **49**, 607 (1991).

[46] A. H. Mueller, Soft gluons in the infinite momentum wave function and the BFKL pomeron, Nucl. Phys. **B415**, 373 (1994).

[47] G. P. Lepage and S. J. Brodsky, Exclusive processes in perturbative quantum chromodynamics, Phys. Rev. D **22**, 2157 (1980).

[48] H. G. Dosch, T. Gousset, G. Kulzinger, and H. J. Pirner, Vector meson leptoproduction and nonperturbative gluon fluctuations in QCD, Phys. Rev. D **55**, 2602 (1997).

[49] T. Lappi, H. Mäntysaari, and J. Penttala, Relativistic corrections to the vector meson light front wave function, Phys. Rev. D **102**, 054020 (2020).

[50] E. R. Berger, A. Donnachie, H. G. Dosch, and O. Nachtmann, Observing the odderon: Tensor meson photoproduction, Eur. Phys. J. C **14**, 673 (2000).

[51] F. Fillion-Gourdeau and S. Jeon, Tensor meson production in proton-proton collisions from the color glass condensate, Phys. Rev. C **77**, 055201 (2008).

[52] R. S. Pasechnik, A. Szczurek, and O. V. Teryaev, Non-perturbative and spin effects in the central exclusive

production of tensor $\chi_c(2^+)$ meson, Phys. Rev. D **81,** 034024 (2010).

[53] J. P. Lansberg and T. N. Pham, Effective Lagrangian for two-photon and two-gluon decays of P-wave heavy quarkonium $\chi(c0, 2)$ and $\chi(b0, 2)$ states, Phys. Rev. D **79,** 094016 (2009).

[54] H.-Y. Cheng, C.-K. Chua, and C.-W. Hwang, Covariant light front approach for s wave and p wave mesons: Its application to decay constants and form-factors, Phys. Rev. D **69,** 074025 (2004).

[55] A. D. Martin, M. G. Ryskin, and T. Teubner, The QCD description of diffractive rho meson electroproduction, Phys. Rev. D **55,** 4329 (1997).

[56] A. D. Martin, M. G. Ryskin, and T. Teubner, Q^2 dependence of diffractive vector meson electroproduction, Phys. Rev. D **62,** 014022 (2000).

[57] I. Babiarz, R. Pasechnik, W. Schäfer, and A. Szczurek, Hadroproduction of scalar P-wave quarkonia in the light-front k_T-factorization approach, J. High Energy Phys. 06 (2020) 101.

[58] R. Fiore and V. R. Zoller, Charged currents, color dipoles and xF(3) at small x, JETP Lett. **82,** 385 (2005).

[59] L. Motyka and G. Watt, Exclusive photoproduction at the Tevatron and CERN LHC within the dipole picture, Phys. Rev. D **78,** 014023 (2008).

[60] I. Babiarz, R. Pasechnik, W. Schäfer, and A. Szczurek, Light-front approach to axial-vector quarkonium $\gamma^*\gamma^*$ form factors, J. High Energy Phys. 09 (2022) 170.

[61] C. R. Ji, P. L. Chung, and S. R. Cotanch, Light cone quark model axial vector meson wave function, Phys. Rev. D **45,** 4214 (1992).

[62] S. N. Gupta, J. M. Johnson, and W. W. Repko, Relativistic two photon and two gluon decay rates of heavy quarkonia, Phys. Rev. D **54,** 2075 (1996).

[63] H. Mäntysaari, K. Roy, F. Salazar, and B. Schenke, Gluon imaging using azimuthal correlations in diffractive scattering at the Electron-Ion Collider, Phys. Rev. D **103,** 094026 (2021).

[64] V. Shtabovenko, R. Mertig, and F. Orellana, FeynCalc 9.3: New features and improvements, Comput. Phys. Commun. **256,** 107478 (2020).

[65] A. Dumitru, H. Mäntysaari, and R. Paatelainen, Stronger C-odd color charge correlations in the proton at higher energy, Phys. Rev. D **107,** L011501 (2023).

[66] F. Schlumpf, Relativistic constituent quark model of electroweak properties of baryons, Phys. Rev. D **47,** 4114 (1993); **49,** 6246(E) (1994).

[67] S. J. Brodsky and F. Schlumpf, Wave function independent relations between the nucleon axial coupling g(A) and the nucleon magnetic moments, Phys. Lett. B **329,** 111 (1994).

[68] K. J. Golec-Biernat and A. M. Stasto, On solutions of the Balitsky-Kovchegov equation with impact parameter, Nucl. Phys. **B668,** 345 (2003).

[69] J. Berger and A. Stasto, Numerical solution of the nonlinear evolution equation at small x with impact parameter and beyond the LL approximation, Phys. Rev. D **83,** 034015 (2011).

[70] T. Lappi and H. Mäntysaari, Single inclusive particle production at high energy from HERA data to proton-nucleus collisions, Phys. Rev. D **88,** 114020 (2013).

[71] H. Kowalski, T. Lappi, C. Marquet, and R. Venugopalan, Nuclear enhancement and suppression of diffractive structure functions at high energies, Phys. Rev. C **78,** 045201 (2008).

[72] P. V. Landshoff, Model for elastic scattering at wide angle, Phys. Rev. D **10,** 1024 (1974).

[73] A. Donnachie and P. V. Landshoff, Elastic scattering at large t, Z. Phys. C **2,** 55 (1979); **2,** 372(E) (1979).

[74] A. Donnachie and P. V. Landshoff, Multi—gluon exchange in pp elastic scattering, Phys. Lett. **123B,** 345 (1983).

[75] A. Donnachie and P. V. Landshoff, p p and anti-p p elastic scattering, Nucl. Phys. **B231,** 189 (1984).

[76] L. D. Landau, On the angular momentum of a system of two photons, Dokl. Akad. Nauk SSSR **60,** 207 (1948).

[77] C.-N. Yang, Selection rules for the dematerialization of a particle into two photons, Phys. Rev. **77,** 242 (1950).

[78] Z. Ye, J. Arrington, R. J. Hill, and G. Lee, Proton and neutron electromagnetic form factors and uncertainties, Phys. Lett. B **777,** 8 (2018).

[79] H. Kowalski, L. Motyka, and G. Watt, Exclusive diffractive processes at HERA within the dipole picture, Phys. Rev. D **74,** 074016 (2006).

[80] Y. Li, M. Li, and J. P. Vary, Two-photon transitions of charmonia on the light front, Phys. Rev. D **105,** L071901 (2022).

[81] W. Kwong, P. B. Mackenzie, R. Rosenfeld, and J. L. Rosner, Quarkonium annihilation rates, Phys. Rev. D **37,** 3210 (1988).

[82] R. Barbieri, M. Caffo, R. Gatto, and E. Remiddi, Strong QCD corrections to p wave quarkonium decays, Phys. Lett. **95B,** 93 (1980).

[83] Y. Li, P. Maris, and J. P. Vary, Quarkonium as a relativistic bound state on the light front, Phys. Rev. D **96,** 016022 (2017).

[84] C. F. von Weizsacker, Radiation emitted in collisions of very fast electrons, Z. Phys. **88,** 612 (1934).

[85] E. J. Williams, Correlation of certain collision problems with radiation theory, Kong. Dan. Vid. Sel. Mat. Fys. Med. **13N4,** 1 (1935).

[86] V. M. Budnev, I. F. Ginzburg, G. V. Meledin, and V. G. Serbo, The two photon particle production mechanism. Physical problems. Applications. Equivalent photon approximation, Phys. Rep. **15,** 181 (1975).

[87] A. Caldwell and H. Kowalski, The J/ψ way to nuclear structure, in *13th International Conference on Elastic and Diffractive Scattering (Blois Workshop): Moving Forward into the LHC Era* (2009), pp. 190–192, arXiv:0909.1254.

[88] Y. Jia, Z. Mo, J. Pan, and J.-Y. Zhang, Photoproduction of C-even quarkonia at the EIC and EicC, Phys. Rev. D **108,** 016015 (2023).

[89] E. C. Aschenauer, S. Fazio, J. H. Lee, H. Mantysaari, B. S. Page, B. Schenke, T. Ullrich, R. Venugopalan, and P. Zurita, The Electron–Ion Collider: Assessing the energy dependence of key measurements, Rep. Prog. Phys. **82,** 024301 (2019).

[90] J. C. Collins and R. K. Ellis, Heavy quark production in very high-energy hadron collisions, Nucl. Phys. **B360,** 3 (1991).

[91] H. Aihara *et al.* (TPC/Two Gamma Collaboration), Formation of spin one mesons by photon-photon fusion, Phys. Rev. D **38,** 1 (1988).

[92] J. Bartels and L. Motyka, Baryon scattering at high energies: Wave function, impact factor, and gluon radiation, Eur. Phys. J. C **55,** 65 (2008).

[93] A. Dumitru, V. Skokov, and T. Stebel, Subfemtometer scale color charge correlations in the proton, Phys. Rev. D **101,** 054004 (2020).

[94] G. Chachamis and A. Sabio Vera, Solution of the Bartels-Kwiecinski-Praszalowicz equation via Monte Carlo integration, Phys. Rev. D **94,** 034019 (2016).

[95] Y. Hatta, B.-W. Xiao, and F. Yuan, Gluon tomography from deeply virtual Compton scattering at small-x, Phys. Rev. D **95,** 114026 (2017).

[96] J. R. Forshaw and M. G. Ryskin, Diffractive vector meson production at large momentum transfer, Z. Phys. C **68,** 137 (1995).